The Sun, Solar Wind, and Magnetic Field

E. J. SMITH

Jet Propulsion Laboratory, California Institute of Technology, Pasadena, CA, USA

1. – Introduction

This seminar is the first of two on the sun and heliosphere. It addresses the sun, solar wind and magnetic field with emphasis on recent observations by the Ulysses mission. Part II addresses the heliosphere and local interstellar medium/LISM, again based, on recent Ulysses results.

Ulysses is a joint mission between NASA and ESA (European Space Agency). The two agencies have about equal responsibilities for the mission with about the same number of U.S. and European scientists participating in the investigations. There are two project scientists. I am the U.S. project scientist and a Co-I Investigator of the magnetic field experiment. Richard G. Marsden is the ESA project scientist and Co-I Investigator of one of the energetic particle experiments. Because of my background in measuring magnetic fields, I have somewhat of a "magnetocentric" point of view and will speak extensively about magnetic fields in the heliosphere, hopefully without giving too little attention to the other major constituents.

The outline of my talk is as follows. I will begin with a brief description of the mission. This approach enables an uninterrupted discussion of the science content which then follows. Rather than assume everyone has adequate background information on the sun and solar wind, I will begin with a discussion of the basic scientific issues. As was true of the earliest historical observations, the background description begins by treating the sun, the corona and the solar magnetic field as homogeneous, i.e., without magnetic structure of any kind. The more realistic case of the inhomogeneous magnetized sun will be treated next leading to the Ulysses observations and their implications.

2. – The Ulysses Mission

The unique aspect of Ulysses [1] is its solar polar orbit which, for the first time, carries a spacecraft far out of the ecliptic plane and enables the investigation of the heliosphere in three dimensions. The launch was in October 1990, approximately 9 years ago, and the spacecraft has since produced essentially continuous measurements. Figure 1 includes the portion of the elliptical orbit near the ecliptic which carried the spacecraft outward to Jupiter at 5.3 AU. The gravitational field of Jupiter was then used to reorient the orbit plane so that it has an inclination to the sun's equator of 80° heliospheric latitude. Given the tilt of the sun's magnetic poles relative to its axis of rotation, this inclination means that all magnetic latitudes are sampled.

After leaving Jupiter, the spacecraft first headed toward the sun's south pole to make optimum use of the available kinetic energy. The elliptical orbit simultaneously carried the spacecraft inward toward a perihelion of 1.3 AU. After reaching the highest south latitude at 2.2 AU, the spacecraft continued to gather speed, returned to the equator and crossed it enroute to the north polar cap.

Figure 2 shows the spacecraft which is spin-stabilized rotating around the axis of the Earth- pointing high gain antenna. Power is derived from a Radioisotope Thermoelectric Generator which converts heat released by radioactive decay of plutonium into electric current. A boom deployed in the plane perpendicular to the spin axis contains two magnetometers, a gamma ray/x-ray detector, plus a magnetic field plasma wave detector (search coil).

The experiment complement is designed to make space plasma measurements almost exclusively. The combined instrument capabilities ensure measurement of all the heliospheric constituents of scientific interest without significant gaps in the particle energies or the frequency of hydromagnetic, plasma or radio waves.

An important consideration is that the observations thus far were carried out at and near sunspot minimum and the minimum in solar activity. The spacecraft is continuing to make measurements after returning to aphelion at 5.3 AU in April 1998. It is intended that high heliographic latitudes will now be surveyed during the approaching maximum in solar activity.

3. – Background: The Homogeneous Sun

The basic theory of the solar wind was derived by Eugene Parker approximately 40 years ago [2]. It was based on two prior developments. A hydrostatic model of the corona extending far into space was developed earlier by S. Chapman to account for observations of a relatively high density plasma surrounding Earth (based on an incorrect interpretation of the Zodiacal light) [3]. A defect of this static model was that the density and pressure remained finite at infinite distance from the sun. The second development was the inference drawn by L. Biermann [4] from a study of comet plasma tails that a steady "solar corpuscular radiation" (a wind) was present at large distances from the sun having a speed of $\sim 10^3$ km/s. Parker's considerable contribution was to develop a

model of the solar wind that overcame the defects of the static model and accounted for the "corpuscular radiation".

Figure 3 is a familiar figure based on Parker's solution of the hydrodynamic equations (ignoring the sun's magnetic field). Four possible solutions are shown representing the rates of the outflow speed of coronal plasma, u, referred to a so-called critical velocity, u_c, i.e., the speed at the critical point or distance $r_c = GM_S m/4kT$. G is the universal gravitational constant, M_S, the solar mass, m, the proton mass, k Boltzman's constant and, T, the proton temperature. The parameter, u/u_c, is shown as a function of radial distance from the sun, r, normalized to r_c. The relevant solar wind solution (class 2) passes through the critical point which, for a typical coronal temperature of 10^6 K, is located at $\sim$ 30 solar radii. The solution designated class 1 leads to the so- called "solar breeze" which is not consistent with observations of the solar wind as it exists at the present. (It may be applicable, however, to the Maunder minimum in sunspot number in the 1600s.) The other two classes of solution can be disregarded as being physically unrealizable. The hydrodynamic solution for a wind originating everywhere in the corona leads to a supersonic wind outside the critical point whose outflow speed greatly exceeds the local speed of sound.

Figure 4 exploits a solar wind analogy based on a rocket engine (flow through a deLaval nozzle) demonstrating its plausibility [5, 6]. Acceleration of the plasma is a basic consequence of gas dynamics in which a hot gas in a combustion chamber (the corona) is able to expand through a constriction or nozzle(solar gravity) and random thermal motion is converted to a directed outflow (wind). Such an analogy played an important role in the early controversy surrounding the Parker theory which involved collective (gas dynamic) motion vs. individual particle (exospheric) motion [7, 8] .

The effect of the wind in carrying off the solar magnetic field was also considered by Parker who assumed that the magnetic field played a passive role and was dominated and controlled by the convective pressure of the wind. Probably because electromagnetism is first experienced in the laboratory and plasma physics is first encountered in the physics of the Earth's magnetosphere, many research workers consider electric fields and currents as fundamental. However, Parker, like many other plasma physicists, is an advocate of the so-called "V-B paradigm" [9]. This approach considers only $\mathbf{V}$ and $\mathbf{B}$ to be of real interest with the electric field being derivable from $\mathbf{E} = -\mathbf{V} \times \mathbf{B}$ (or, alternately, being eliminated from consideration by a suitable coordinate transformation) and the current from $\mathbf{j} = \nabla \times \mathbf{B}/\mu_0$. The relevant forces then become plasma pressure and magnetic field pressure and tension (the Maxwell stresses). One of the most influential advocates of the opposing viewpoint for many years was H. Alfvén, who persistently asked the question: "How do the currents close?"

There is probably no resolution to the question of which approach is "correct". Either approach is acceptable if it leads to the correct result. If both approaches are applied and lead to consistent results, some degree of confidence is gained. It should be recognized, however, that in many cases the V-B paradigm leads to simpler solutions. An example is its use by Parker to derive the spiral magnetic field. (Electric fields and currents do not appear in any of the derivations in Parker's book on the solar wind and interplanetary

dynamics).

Figure 5 shows the solar wind velocity streamlines and parallel magnetic field lines in a frame of reference corotating with the sun in which the electric field vanishes. The solar wind velocity has a radial component, V_r, and an azimuthal component, $-\Omega r$, in standard spherical coordinates. For simplicity, the view is in the equatorial plane corresponding to $\theta = \pi/2$. At other latitudes, the azimuthal component is $-\Omega r \sin\theta$ and the field lines spiral around on the surface of a cone.

The magnetic field lines have the same shape in both the rotating and inertial frames. This is a consequence of the special theory of relativity for $V_r \ll c$ where c = the velocity of light. The tangent of the angle between the field direction and the radial direction, called the Parker spiral angle, is $\tan\phi_P = B_\phi/B_r = -\Omega r \sin\theta/V_r$. The locus of the field line is derivable from the azimuthal and radial differentials which, at the equator, is given by $r\,d\phi/dr = -\Omega r/V_r$. Hence, $\phi = -\Omega r/V_r$, the equation of an Archimedes spiral. It is noteworthy that, ϕ, the longitude angle to the end of the field line at the sun is equal to $\tan\phi_P$.

If this approach is not used, the Parker spiral can be derived from consideration of the electric field in inertial space, i.e., $\mathbf{E} = -\mathbf{V} \times \mathbf{B}$. This relation, commonly described as the "frozen" field condition with the field co-moving with the plasma, derives from the transformation of an electric field in an inertial frame, $\mathbf{E}$, into $\mathbf{E}'$ in a frame moving with velocity $\mathbf{V}$: $\mathbf{E}' = \mathbf{E} + \mathbf{V} \times \mathbf{B}$. In a collisionless, infinitely conducting plasma, $\mathbf{E}' = \mathbf{0}$ so that $\mathbf{E} = -\mathbf{V} \times \mathbf{B}$ as above. Basically, a magnetic field component will be induced in the plasma that will make $\mathbf{E}' = \mathbf{0}$.

Applied to the rotating sun as a plasma (infinite conductor) in motion, there is an electric field in inertial space given by $\mathbf{E} = -\Omega r \sin\theta B_r \hat{\mathbf{e}}_\theta$ (northward in spherical coordinates whose pole is parallel to the solar rotation axis, $\mathbf{\Omega}$). The electric field associated with the motion of the solar wind at the same point of observation is $\mathbf{E} = V_r B_\phi \hat{\mathbf{e}}_\theta$. Since only one electric field is possible, the two must be equal and $V_r B_\phi = -\Omega r \sin\theta B_r$ giving the same result as above, $\tan\phi_P = B_\phi/B_r = -\Omega r/V_r$.

The global configuration of the magnetic field based on the Parker model (again, as seen projected into the solar equator) is shown in Figure 5 for $V_r = 300$ km/s. The solar wind flow is radial while the field lines form spirals analogous to those commonly formed by the water drops from a rotating lawn sprinkler.

If allowance is made for the tilt of the sun's magnetic pole, or for a homogeneous magnetic field with B_r independent of latitude but with opposite polarization or senses in the two heliospheres, half of the fields will point radially outward and half inward as indicated by the direction of the arrowheads in the figure. The two half circles then correspond to "magnetic sectors", one "plus" the other "minus", and a pair of boundaries, marked S/B for "sector boundary", representing the transitions for one sector to the other (+/-, - /+) [10]. Physically, the S/B corresponds to a sheet current which will be discussed subsequently.

4. – Background, the Inhomogeneous Sun

Observations over many years have revealed that the solar wind does not issue from all over the sun simultaneously as assumed in the discussion above. The basic reason is that the sun's magnetic field does not play a passive role but actually dominates the outflow. When the earliest measurements of the solar wind and magnetic field at 1 AU were extrapolated back to the sun, assuming conservation of magnetic flux, the energy density of the field was found to be larger than the energy density of the coronal plasma [11].

This realization indicated that, if the field is transverse to the radial direction, it can prevent the outflow. Generally, this condition obtains at low solar latitudes where the magnetic field lines tend to be parallel to the Sun's surface and take the form of magnetic loops which begin and end on the surface. This configuration gives rise to so called magnetic "arcades" and to the associated "streamers" which are commonly seen when the corona is viewed in white light at eclipses or with coronagraphs. These bright features are the result of visible radiation from the surface being scattered by electrons trapped on these "closed" field lines. Generally, these structures extend around the sun to form the streamer belt or coronal disc.

On the other hand, regions in which the magnetic field is vertical, or directed radially outward, will assist rather than oppose the coronal outflow. When the solar wind leaves such a source region, the field lines are carried off by the wind and their possible connection to the sun at the other end of the field line is lost. Such field lines with only one end attached to the sun are termed "open".

There is now a large body of evidence to show that the steady solar wind issues from open field regions. A particularly clear instance of this is the association of fast solar wind streams with polar coronal holes, i.e., regions overlaying the polar caps that appear dark in IR, visible, UV or x-ray wave lengths as a result of the density depletion accompanying the outflow [12]. Coronal holes are not restricted to the polar caps but can extend downward to cross the equator or can also appear as "equatorial" coronal holes without any attachment to the polar regions.

The magnetic fields captured by the solar wind or obstructing the flow are those having a large enough scale to extend from the surface into the corona. Their magnitudes are typically a few Gauss. They are not the strong kilogauss fields associated with sunspots and active regions.

The continued presence of magnetic sectors in/near the ecliptic is evidence of the dominance of solar wind magnetic fields by the sun's polar caps or by the largest scale field component equivalent to a dipole. Fast streams from north and south polar coronal holes have opposite magnetic polarities corresponding to the sense of the field in the polar caps. At present, e.g., the field is outward in the north polar region and the fast streams from the north polar coronal hole are positive (outward) and vice-versa for streams from the south.

The persistence of the sector structure is demonstrated by Figure 6 containing observed polarities over successive 27d solar rotations during the solar maximum in 1979.

Note the two sector pattern throughout the 2-1/2 years which is not disrupted in spite of a large number of transient events occurring on the sun at that time and the reversal in polarity of the polar magnetic fields.

Many of the above properties are shown schematically in Figure 7, a 3D view of the magnetic field within a few radii of the sun. The rotation axis, $\mathbf{\Omega}$, and the magnetic axis, $\mathbf{M}$, are tilted relative to one another [13]. Open field lines from the north polar cap are shown as descending to low latitudes (see below where the Ulysses results are discussed) and passing above the current sheet (or sector boundary) which contains a warp reminiscent of a hat brim. Closed field lines beginning and ending on the sun are also shown in the region defined by the inner edge of the current sheet. Field lines originating from the south are shown with an opposite polarity. The existence of the current sheet is required by Maxwell's equations applied to the boundary between these oppositely directed fields.

As the sun rotates, $\mathbf{M}$ revolves around $\mathbf{\Omega}$ and the current sheet wobbles up and down. Continued outflow of the solar wind produces a current sheet that extends to great distances from the sun. The effect of the wobble in $\mathbf{M}$ is to produce a periodic series of peaks and troughs as shown in the accompanying representation (Figure 8). As the current sheet rotates past the spacecraft, fields above and then below it are sampled resulting in the observed sector structure.

Because of the continued spiraling of the magnetic field, the field direction changes from being nearly radial near the sun to being nearly azimuthal (wound up like a clock spring) at large distances. Since Maxwell's equations imply that the direction of current flow in the current sheet is transverse to the adjacent fields, the current changes from azimuthal to radial with increasing distance. It is an interesting exercise to compute the currents in the current sheet and surrounding the sun (as a consequence of the spiraling of the field at all latitudes) and to compare them [14]. This example also illustrates the point made above about how, having found $\mathbf{B}$ (using the VB paradigm), the currents can be determined.

Consider a simple geometry in which $\mathbf{\Omega}$ and $\mathbf{M}$ are aligned (no warps) so spherical polar coordinates can be used. The components of $\mathbf{B}$ are known from conservation of magnetic flux and the spiral angle. Thus, $B_r = B_0 r_0^2/r^2$ where the subscript zero refers to a reference radius, nominally 1 AU. It is assumed that B_r at the sun's surface is independent of latitude, again for simplicity. (This assumption is not as unrealistic as it might appear as will become evident from Ulysses observations presented below).

The Parker spiral implies that $B_\phi = -B_0 r_0 \cos\delta/r$ where δ is the heliographic latitude and $\Omega r_0/V = 1$ has been assumed (a condition satisfied on average at 1 AU). The field is assumed to be outward in the north so the above equations are appropriate to the north hemisphere. The field in the south hemisphere is then inward, so the signs of B_r and B_ϕ are reversed.

The current densities are derivable from the known fields. Above and below the current sheet, $\mathbf{j} = \nabla \times \mathbf{B}/\mu_0$ which works out to be $J_R = -2B_0 r_0 \sin\delta/\mu_0 r^2$, $J_\phi = 0$, $J_\delta = 0$ in both the north and south heliosphere. Thus, inward radial currents responsible for the B_ϕ component associated with the spiraling, are present throughout space (except

for the current sheet) and are actually largest over the poles.

The linear current density, $\mathbf{K}$, in the current sheet is derivable from the Maxwell boundary condition which states that $\mathbf{K} = \triangle\mathbf{B}$. Thus, $K_r = 2B_0 r_0/\mu r$ and $K_\phi = 2B_0 r_0^2/\mu_0 r^2$ with the radial component falling off more slowly with distance. The direction of current flow, represented by the current streamlines, can be obtained from $r d\phi/dr = K_\phi/K_r = r_0/r$.

Integration results in $\phi r = -r_0$, the equation of a hyperbolic (reciprocal) spiral. The character of this spiral is shown in Figure 8 and is everywhere transverse to the associated Archimedes spiral field. (The Archimedes spiral rotates clockwise opposite in sense to the current.) The development of a non-zero radial current component is evident as the distance increases.

How do these distributed inward currents and the outward sheet current compare? The sum of the inward currents is $I_r = 2\int_0^{\pi/2}\int_0^{2\pi} j_r \cos\delta\, r^2\, d\phi\, d\delta = -4\pi B_0 r_0/\mu_0$. (For $B_0 = 3.5 \times 10^{-9}$ T at 1 AU, $I_{r_0} = 5 \times 10^9$ amp.) The outward current contained in the current sheet is given by $I_r = \int_0^{2\pi} K r_0 r\, d\phi = 4\pi B_0 r_0/\mu_0$. Thus, the two currents compensate and the net flow is zero. (This solution answers the Alfvén question, how and where do the currents close?

The geometry of the Heliospheric Current Sheet (HCS), and its presence or absence at a specific location, is of interest because it tends to organize important plasma and energetic particle properties in the solar wind. Figure 9 shows the results of a superposed epoch analysis in which the key "date" is the passage of the current sheet. As seen, the density of the solar wind peaks while the speed and temperature reach minima at the current sheet. Regarding the energetic particles, a correlation between changes in the inclination of the current sheet and the intensity of galactic cosmic rays has been demonstrated.

The current sheet itself is very thin on a scale appropriate to most structures in the solar wind. Current sheet crossings typically occur in a few minutes and are equivalent to a thickness of 10^5km [15]. (Features having smaller scales, such as shocks or hydromagnetic discontinuities are considered to be a form of microstructure.)

In the interest of accounting for the observed sector structure in terms of observed magnetic fields, a technique has been devised for projecting photospheric fields onto a so-called source surface [16, 17]. Figure 10 is a schematic representation of the technique. Currents are assumed to be absent in the corona so that the fields observed by Earth-based magnetographs can be extrapolated outward assuming they can be described by a scalar potential. A boundary condition is then applied at a spherical outer shell requiring that the fields beyond that shell become radial.

As shown, small scale closed magnetic fields do not reach the "source surface". A wavy line is found on this surface across which the field polarity changes (the radial field vanishes). This "neutral line" is customarily identified with the HCS at larger distances. The distance to the radial outer shell is chosen to maximize the correlation between the source surface neutral lines and observed sector boundaries, resulting in a location of $\sim 2.5 r_S$. The source surface is undoubtedly a fiction but the concept has proven useful and, no doubt, there is a surface (probably not at all spherical) along which the

magnetic field is radial. (Ulysses observations have shown stresses are present between the photosphere and this surface so that that the absence of currents in/above the corona cannot be correct. See below).

5. – Ulysses Observations of the Sun, Solar Wind and Magnetic Field in 3-D

This section presents some of the more important findings of the Ulysses spacecraft as it traveled from the ecliptic to the sun's poles. (Limitations of space and time prohibit a more comprehensive review and it has been necessary to be selective. For topics not covered here, the interested reader should consult the several special issues of journals and the individual publications based on Ulysses results for which the references in this article serve as a starting point).

The solar wind speed and density measurements during the "fast latitude scan", when the spacecraft traveled from $-80°$ to $+80°$ latitude in only 6 months, appear in Figure 11 [18]. The band centered on the equator shows the limited range of latitudes covered by spacecraft measurements made previously in the ecliptic and serves to illustrate the large extent by which our knowledge has been increased.

The speed measurements distinguish two different states of the solar wind, a high-speed ($\sim$ 800 km/s) wind at high latitudes (above 20 - 30°) and a slow, low latitude wind straddling the solar equator. Another important discriminator is a large amount of variability in the speed and density at low latitudes. There are large increases and decreases in V and nr^2 (the density is normalized at the point of observation by multiplying by r^2 on the basis of conservation of mass).

The normalized plasma density is seen to be independent of latitude in the high- speed wind. The density is higher in the low-speed region, a result consistent with a well-known anticorrelation between n and V (or approximately constant flux density, nV) over the entire range of latitudes.

Some of the variance is intrinsic to the slow wind but the largest excursions are caused by fast wind overtaking slower wind that left the sun earlier. To a considerable extent, these "fast stream-slow stream" or "stream-stream" interactions are the result of the tilt of the magnetic dipole to the sun's rotation axis which can bring fast wind down into the ecliptic at certain solar longitudes so that the over-taking occurs. The fact that the maximum speeds at low latitude are typically less than $\sim$ 800 km/s is probably the consequence of two effects: (1) the existence of a finite gradient in solar wind speed with latitude (which for low tilt angles does not allow the fastest high latitude wind to tip down into the ecliptic) and (2) the basic effect of the interaction which leads to an acceleration of the slow wind and a deceleration of the fast wind.

Another solar wind parameter of interest (and one which has proven a difficult challenge for solar wind acceleration models) is the temperature. The proton temperature averaged over time and the anisotropic temperature parallel and perpendicular to $\mathbf{B}$, i.e., $T = 2T_\perp/3 + T_\parallel$, is shown in Figure 12 as a function of radial distance. The lower branch (March 1991) is for data acquired enroute to Jupiter showing that T remained basically constant at low latitude (consistent with prior Pioneer and Voyager measurements). The

upper branch shows an increasing temperature with increasing latitude (refer to the upper scale) and decreasing distance. The temperature increases with increasing latitude and speed and is essentially consistent with a well established correlation between V and T that holds in/near the ecliptic.

The measurement of heavy ions by one of the Ulysses experiments, the Solar Wind Ion Composition Spectrometer or SWICS, yields information on mass (composition), velocity (including thermal velocity or temperature) and charge state (degree of ionization of atoms such as C, O, etc.) [19]. By comparing the relative abundances of different charge states of a specific species, e.g., fractional abundance of O^{7+}, O^{8+}, the coronal temperature at which the ionization is "frozen-in" and is then unchanging as the solar wind leaves the corona can be derived. Figure 12 contains simultaneous measurements of the solar wind speed (in terms of α particles rather than protons, V_α) and the freezing-in temperature of oxygen, T_O [20]. The plot of V_α identifies the transition from low latitude, low speed wind to high latitude, high speed wind. There is an observed anticorrelation between T_O and V_α showing that the freezing-in temperature is lower in the fast wind than in the slow wind (recall, however, that the fast wind is hotter than the slow wind). The lower values of T_O in the fast wind are consistent with the heavier solar wind ions originating further out in the corona than those constituting the slow wind.

The composition measurements available from SWICS reveal another significant difference between the fast and slow winds. Figure 12 also contains V_α and $T_O(O^{6+}/O^{7+})$ averaged over several solar rotations which serve to distinguish fast wind (at the beginning and end of the plot) from slow wind (middle of the plot). The abundances of the two wind types is represented by the ratio of the amount of magnesium to that of oxygen, Mg/O. As is evident, the freezing-in temperature and the Mg/O ratio are closely correlated and show that the composition of the fast wind is deficient in magnesium as compared to the slow wind.

Magnesium is representative of elements having a low ionization potential, in contrast, for example, to the noble gases, such as He, Ne or A. Measurements by in-ecliptic spacecraft in years past have demonstrated an effect called the First Ionization Potential/FIP effect which is represented in the Ulysses data by Figure 13. The relative abundance of many heavy elements, from He through Fe, referred to the abundance of oxygen in the solar wind and in the photosphere, is shown as a function of First Ionization Time (which is directly related to the FIP). Two branches are apparent, the upper one corresponding to slow (interstream) wind and the lower branch to fast (coronal hole) wind. Although there is a general reduction in the FIP effect in the fast wind, the effect of the ionization potential of the heavy elements is still evident. Since the FIP effect is characteristic of the solar chromosphere, this result indicates some sort of coupling between the high corona in which the heavy ions are frozen into the fast solar wind and the lower lying chromosphere. This result may not be too surprising in view of the fact that the observed solar wind mass flux averaged over all latitudes requires that the solar corona be replenished several times a day. Thus, there must be a flow of mass from below into the corona as well as a transfer of heat (a condition that is absent from many, although not all, solar wind models).

We now turn to Ulysses observations of the magnetic field. One of the chief findings is represented by Figure 14 in which daily averages of the radial field component, B_r, multiplied by the square of the radial distance (to correct for the radial gradient assuming conservation of magnetic flux) are shown as a function of time (below) and latitude (above) [21]. The dashed vertical lines identify regions of structure-less fast wind from the structured slow wind. The most obvious feature is the change in sense from negative (inward) fields in the south to positive (outward) fields in the north, consistent with the polarities of the two polar caps. The other important feature is that in the fast wind $B_r r^2$ does not depend on latitude. In fact, comparison with simultaneous in-ecliptic measurements shows that $B_r r^2$ on average is essentially unchanged from the equator to the pole.

This simple result has profound implications for the solar wind and implies the strength of the sun's polar field. Measurements by solar magnetographs on Earth reveal a dipole-like character to the largest scale photospheric magnetic field implying that the field strength increases from the equator the pole. On this basis, the source surface models, discussed above, predicted a significant increase in B_r with increasing latitude, contrary to the Ulysses observations. This apparent contradiction means that the strong polar cap magnetic fields are being redistributed as the solar wind flows outward, achieve a uniform distribution at some distance from the sun and thereafter remain uniform [21, 22].

The dominance of the magnetic field energy density in the corona mentioned above provides an explanation for this phenomenon. The magnetic pressure, $B^2/8\pi$, is much larger over the poles than at low latitudes and exerts a force on the solar wind pushing it toward lower latitudes as it flows outward. If the magnetic pressure is dominant, it will be expected to finally reach an equilibrium or relaxed state in which the pressure and B_r are uniform with latitude.

This non-radial flow (absent, e.g., in the Parker model) is also evident in the low latitude of $\sim 30°$ reached by the fast wind from the coronal holes which have observed equatorward boundaries of $\sim 70°$ latitude. Thus, the fast solar wind driven by a magnetic force expands non-radially by a factor of 5-6 in solid angle or in the areas on a sphere centered on the sun. Knowledge of this expansion factor combined with the observed magnetic flux, $B_r r^2$, leads to an estimate of the sun's polar field strength of ~ 7 Gauss. Theoretical consideration of the time required to achieve a uniform magnetic field implies that B_r is constant by ~ 5 solar radii. Curiously, the surface along which B_r = constant corresponds to the Parker field for a homogenous sun described above so that many of the above considerations and derivations are still applicable. (Of course, the existence of the solar wind at low latitudes combined with the tilted magnetic dipole leads to interactions not contemplated in the simplest version of the Parker model.)

Other aspects of the magnetic field also conform reasonably well to Parker's magnetic field. In Figure 14, the middle panel, designated azimuth angle, ϕ_B, contains information on the Parker spiral [23]. The smooth curve passing through the variable data points is the Parker spiral, ϕ_P, where measured values of V_r were used and the angular velocity, Ω_0, is the equatorial sidereal rotation rate of 25.4 days. The data points are for the

observed spiral angle, $\phi_B = \tan^{-1}(B_\phi/B_r)$. The gradual increase in both ϕ_P and ϕ_B toward 180° at 80° south and approaching 360° near 80° north are evidence that the field is essentially radial at maximum latitude just as predicted by the Parker model.

The upper panel shows the observed latitude angle of the field, $\delta_B = \sin^{-1}(B_\theta/B_r)$. In spite of the large dispersion in the values, the average value is seen to be zero. This result is also consistent within the Parker model in which the absence of a north-south component is the result of the strictly radial flow assumed in the model. (It is not assumed to be zero as is occasionally claimed in the literature.)

Finally, the bottom panel shows the variance in field magnitude, $|B|$, along the orbit with 0° latitude corresponding approximately to perihelion, the closest approach to the sun (1.3 AU) since launch. (It should be noted that the root mean square value of the magnitude is shown derived from instantaneous values of $|B|$ so that it includes a contribution from ever-present fluctuations in the field direction.)

The variances in B_r, ϕ_B and δ_B are not the result of noise associated with the magnetometer. The fluctuations are real variations in the field which are present on essentially all time scales [24]. Comparison with $|B|$ shows that the changes are principally in direction not magnitude.

This brief discussion of the ever-present fluctuations in the magnetic field (variously described as discontinuities, waves and/or turbulence) serves to introduce another characteristic of the high-speed wind, namely, the continuous presence of large amplitude Alfvén waves [25, 26]. Such waves are commonly observed in the ecliptic, often in association with fast streams, and their properties are well established. The means of identification is the basic relation between vector changes in the solar wind velocity, $\delta\mathbf{V}$ and magnetic field, $\delta\mathbf{B}$, which (for isotropic pressure/temperature) is simply $\delta\mathbf{B} = \pm\delta\mathbf{V}/(4\pi nM)^{\frac{1}{2}}$, where M is the average mass of the plasma and n is the density.

The plus/minus sign is important because it identifies the direction of propagation with respect to the ambient field, $\mathbf{B}$. The Poynting vector, $\mathbf{k}$, has the direction of $\delta\mathbf{E} \times \delta\mathbf{B}$, i.e., the cross product of the changes in the electric and magnetic fields. Since $\delta\mathbf{E} = -\delta\mathbf{V} \times \mathbf{B}$, $\delta\mathbf{V}$ parallel to $\delta\mathbf{B}$ implies $\mathbf{k}$ is antiparallel to $\mathbf{B}$ and is associated with the plus sign (as a simple diagram showing the relation between these vectors shows). An anti-correlation of $\delta\mathbf{V}$ with $\delta\mathbf{B}$ (the minus sign) indicates propagation along $\mathbf{B}$.

The appearance of these Alfvén waves in the fast wind is seen in Figure 15 which contains panels for the three components of $\mathbf{B}$ and $\mathbf{V}$ with the magnitude and speed at the bottom. The two middle panels for the two transverse components (east-west and north- south) show the high degree of correlation typically found. The poorer correlation between δB_R and δV_R and their smaller amplitudes of fluctuation imply that the waves tend to be propagating in the radial direction, a conclusion borne out by a principal axis analysis of the three field variances. The lowest panel shows that $|B|$ is approximately constant, another condition characteristic of Alfvén waves, in spite of the large variances which are of order $\delta B/B \approx 1$.

The two middle panels show that $\boldsymbol{\delta}\mathbf{V}$ and $\boldsymbol{\delta}\mathbf{B}$ are in-phase corresponding to the plus sign in the above equation. The data were acquired in 1994 when Ulysses was at a high southern latitude and the ambient field was directed inward. Hence, the waves are

propagating outward away from the sun.

The tendency for Alfvén waves to propagate outward has led to a discussion of their possible contribution to the acceleration of the solar wind, since they represent a component of outward pressure. The Ulysses observations have been combined with a model based on a WKB approximation to extrapolate the wave amplitudes back to the solar wind source region. The results imply that the waves do not contribute significantly to acceleration of the solar wind [25]. (This calculation ignores possible heating of the wind if the waves are damped.)

The normalized correlation coefficient between the transverse field and velocity components is shown over a full range of latitudes in Figure 16. Six years of measurements are represented during which the spacecraft traveled from the equator to $-80°$, back to the equator, to $+80°$ and returned to the equator at 5.3 AU, i.e., one complete orbit about the sun. The correlation coefficient is seen to increase monotonically to very high values near ± 1.0 at high latitude. The rapid change between values of 0.8 and -0.8 coincides with the fast latitude scan. The change of sign is associated with the change in polarity of the ambient field from inward to outward and is consistent with outward propagating Alfvén waves in both solar hemispheres.

6. – Summary

The Parker theory of the solar wind is appropriate to a homogeneous corona in which the gas pressure is dominant, the solar wind flow is radial and the magnetic field is treated simply as a "tracer" in the solar wind. In spite of such simplifications, the model successfully predicts many average properties of the plasma and field. In particular, the field direction agrees reasonably well with the direction corresponding to the Parker spiral implying that the field lines are connected at one end to the rotating sun.

However, observations in the ecliptic over many years, now extended to essentially all latitudes by Ulysses, reveals the important role played by the inhomogeneous magnetic field in the specific regions on the sun in which the solar wind originates. During the broad minimum in solar activity, the fast solar wind issues from regions dominated by open magnetic fields which exert a significant force on the plasma causing it to expand equatorward and to depart from strictly radial flow near the sun.

The Ulysses mission has produced an unprecedented view of the fast solar wind issuing from the polar regions and has revealed many of its essential properties which distinguish it from the slow low latitude wind. The fast wind is hotter and less dense and exhibits a degree of ionization of the heavier elements that implies a lower "freezing-in" temperature at the source. The abundances of the heavier elements are also different than for the slow wind and a coupling with the lower altitude chromosphere is implied by a dependence on the first ionization potential. The fast wind is also characterized by the continuous presence of large amplitude Alfvén waves propagating outward from the sun.

It must be recognized that the above description, emphasizing the Ulysses results, is relevant only to conditions near solar minimum when the sun and solar wind are in their simplest states with a quiescent corona, a well-developed dipole magnetic field and large

coronal holes covering both polar caps. It is to be expected that solar maximum conditions will be drastically different with a dynamic corona, a highly structural magnetic field dominated by high order multipoles and transient coronal holes and the production of numerous coronal mass ejections/CMEs. It is now the task of Ulysses to characterize these phenomena at all latitudes at solar maximum.

* * *

The invitation to participate in this distinguished series and the support provided by the Italian Physical Society is greatly appreciated. Bruno Coppi was a constant source of encouragement. Joyce Wolf provided indispensable support in this age of computers in which more of the burden in preparing manuscripts falls on the author. Portions of this report present work done at the Jet Propulsion Laboratory of the California Institute of Technology for the National Aeronautics and Space Administration.

REFERENCES

[1] MARSDEN R. G, SMITH E. J., COOPER J. F., TRANQUILLE C., *Astron. Astrophys.*, **316** (1996) 279.
[2] PARKER E. N., *Interplanetary Dynamical Processes* (Wiley-Interscience, New York) 1963.
[3] CHAPMAN S., *Smithsonian Contrib. Astrophys.*, **2** (1957) 1.
[4] BIERMANN L., *Zeit. Astrophys.*, **29** (1951) 274.
[5] CLAUSER F. H., *The aerodynamics of mass loss and mass gain of stars*, John Hopkins U. Lab. Report AFOSR TN 60-1386, 1960.
[6] BRANDT J. C., *Introduction to the Solar Wind* (W.H.Freeman & Co., San Francisco) 1970.
[7] CHAMBERLAIN J. W., *Astrophys. J.*, **133** (1960) 47.
[8] CHAMBERLAIN, J. W., *Astrophys. J.*, **133** (1961) 657.
[9] PARKER E. N., *J. Geophys. Res.*, **101** (1996) 10,587.
[10] WILCOX J. M. and NESS N. F. , *J. Geophys. Res.*, **70** (1965) 5793.
[11] DAVIS L., JR., *Models of the interplanetary fields and plasma flow* in *The Solar Wind, Pasadena, California* (Pergamon Press, New York) 1964.
[12] ZIRKER J. B., Ed. *Coronal Holes and High Speed Wind Streams* (Colorado Associated University Press, Boulder, CO) 1977.
[13] SMITH E. J., *The sun and interplanetary magnetic field*, in *The Sun in Time*, edited by C. P. SONETT, M. S. GIAMPAPA, and M. S. MATTHEWS (Univ. of Arizona Press, Tucson) 1991.
[14] SMITH E. J., TSURUTANI B. T. *et al.*, *J. Geophys. Res.*, **83** (1978) 717.
[15] WINTERHALTER D., SMITH, E. J. *et al.*, *J. Geophys. Res.*, **99** (1994) 6667.
[16] ALTSCHULER M. D. and G. NEWKIRK, JR., *Solar Phys.*, **9** (1969) 131.
[17] SCHATTEN K. H., WILCOX J. M. *et al.*, *Solar Phys.*, **70** (1969) 5793.
[18] PHILLIPS J. L., BAME S. J. *et al.*, *Geophys. Res. Lett.*, **22(23)** (1995) 3301.
[19] GLOECKLER G., GEISS J. *et al.*, *Astron. Astrophys. Suppl. Ser.*, **92** (1992) 267.
[20] GEISS J., GLOECKLER G. *et al.*,. *Science*, **268** (1995) 1033.
[21] SMITH E. J. and BALOGH A., *Geophys. Res. Lett.*, **22** (1995) 3317.
[22] SUESS S. T. and SMITH E. J., *Astron. Astrophys.*, **316** (1996) 304.
[23] FORSYTH R. J., BALOGH A. *et al.*,. *J.Geophys.Res.*, **101(A1)** (1996) 395.
[24] FORSYTH R. J., HORBURY T. S. *et al.*,. *Geophys.Res.Lett.*, **23(5)** (1996) 595.
[25] SMITH E. J., BALOGH A. *et al.*, *Geophys. Res. Lett.*, **22** (1995) 3381.

[26] JOKIPII J. R., KÓTA J. *et al.*, *Geophys.Res.Lett.*, **22(23)** (1995) 3385.
[27] HUNDHAUSEN A. J., *Coronal Expansion and Solar Wind* (Springer-Verlag, New York) 1972.
[28] BORRINI G. *et al.*, *J.Geophys.Res.*, **86** (1981) 4565.
[29] FORSYTH R. *et al.*, *Astron. Astrophys.*, **316** (1996) 287.

Fig. 1. Ulysses trajectory [1]. The spacecraft was launched in October 1990 into an ellipse near the ecliptic plane that carried it to an encounter with Jupiter in February 1992. The subsequent gravity assist canceled the spacecraft's azimuthal velocity leaving it in another ellipse highly inclined to the ecliptic/ solar equator. The spacecraft travels clockwise in the figure after leaving Jupiter to reach the south polar cap, designated by the shaded cone, and then proceeds rapidly across the equator to the north polar cap.

Fig. 2. The Ulysses spacecraft. The main features are the high gain antenna mounted above the body of the spacecraft and several appendages: a boom containing the magnetometer sensors and two other experiment sensors, the Radioisotope Thermoelectric Generator power source and two plasma/radio wave antennas (one perpendicular and another parallel to the spin axis).

Fig. 3. Hydrodynamic solutions for an expanding corona [2]. Parker found four classes of solutions as shown. Class 2 represents the supersonic solar wind solution passing through the critical point, at which the convected speed equals the sound speed, and continuing to accelerate as it flows away from the sun.

Fig. 4. Rocket analogy to the generation of the solar wind [6]. The hydrodynamic expansion of the wind to supersonic speeds was highly controversial when first presented. Many physicists considered the plasma to be a collection of individual particles (an exospheric approach). Others correctly noted that a fluid dynamic approach would lead to the heat energy being converted to outflow by the presence of a nozzle, which they identified with the sun's gravity.

Fig. 5. Solar wind streamlines and magnetic field lines [27]. The frame of reference is corotating with the sun. If the magnetic field is assumed to rotate with the sun, the streamlines of the outflowing plasma are parallel to the field lines and the E field vanishes. If an alternative point of view is adopted, the field is not corotating and the motion of the conducting solar atmosphere causes an electric field which is canceled inside the sun by a quadrupole distribution of electric charge. There is then an electric field outside the sun given by $\mathbf{E} = -\mathbf{V} \times \mathbf{B}$ and the field lines still conform to the spirals. This solution to the classic problem of the unipolar inductor is found in many books on plasma physics.

Fig. 6. Magnetic field lines, solar wind flow and magnetic sectors in the inertial frame [2]. The spiraled magnetic field lines are the same in the inertial and corotating frames although the solar wind is radially outward in this frame as indicated by the arrows. The dashed circle represents a radial distance of 1 AU and the plus (minus) signs indicates that the field polarity is outward (inward). A pair of field lines on opposite sides of the sun designated as S/B are the boundary between the two opposite- polarity sectors.

Fig. 7. Sector structure over several years near solar maximum. The format of this figure is commonly used in displaying sector structure. The rows correspond to 27 day solar rotations with a +, - or null symbol assigned to each day, in this case, the day number of a Bartels rotation. Successive rows then show many rotations from years 1974 to 1982. Measurements are shown at two spacecraft locations: IMP/ISEE-3 at 1 AU and Pioneer 11 travelling away from the sun from 3.2 to 11.1 AU. The year and Bartels Rotation (BR) numbers form the leftmost columns. At the extreme right are the year and heliographic latitude of Pioneer 11. Note the similarity of the sector structure in the

two columns showing its persistence to large distances. The interval includes sunspot maximum (1979) during which the sector structure persisted without being disrupted by the increased solar activity.

Fig. 8. Magnetic field lines and current sheet near the sun [13]. The sun's magnetic axis is shown tilted relative to the rotation axis, a typical situation. Two types of field line are shown, closed fields originating at low latitude and open fields from higher latitudes. The open field lines have outward polarities in the north and inward polarities in the south. Where they lie near one another, they are separated by the current sheet which is shown as shaded and warped like a hat brim (or ballerina skirt).

Fig. 9. Global configuration of the heliospheric current sheet. The current sheet shown in figure 8 near the sun actually extends throughout the heliosphere. Figure 7 shows the persistence of the current sheet which is equivalent to the persistent sector boundaries. The solar wind transports the current sheet outward as shown in this figure and the tilt of the HCS to the sun's rotation axis gives rise to a peak and valley which spiral around the sun. Theorists have suggested that the field lines should reconnect across the current sheet disrupting it but measurements out to large distances (Figure 7 and now measurements out to 60 AU) show that the HCS persists.

Fig. 10. Current streamline of the heliospheric current sheet. A single streamline is shown although the current is actually continuous. The magnetic field lines spiral in the opposite sense as in figure 6. As the spiral field becomes increasingly azimuthal with distance, the current becomes increasingly radial. Thus, there is a large net outward radial current in what is equivalent to the magnetic equator of the heliosphere. This outflow is compensated by inward radial currents above the current sheet associated with the spiraling of the field.

Fig. 11. Variation of solar wind parameters around the current sheet [28]. Basic solar wind parameters undergo characteristic changes adjacent to the HCS. In this superposed epoch analysis, the density is seen to increase significantly, while the speed and temperature both reach minima. These properties and a correlation with the coronal streamer belt (coronal disk) show that the current sheet maps back to this persistent solar feature. Some investigators refer to the current sheet as the streamer belt and consider it as simply extending outward from the sun. This structure has also been called the Heliospheric Plasma Sheet. The use of "sheet" is acceptable because the plasma and field change on scales which are very thin compared to the dimensions of the heliosphere.

Fig. 12. The solar wind magnetic field emanating from a source surface [17]. The inner circle represents the sun, the view is perpendicular to the rotation axis and photospheric field lines are shown schematically. The dashed circle represents the source surface at which any field lines crossing it become radial. Strong but smaller scale fields typical of active regions do not reach the source surface but remain closed. Beyond the source surface, the field gradually develops its characteristic spiral form. The sector structure is indicated.

Fig. 13. Solar wind speed and density from pole to pole [18]. The upper data plot shows the relatively structureless wind with speeds in excess of 700 km/sec above $\pm 20°$ latitude. At lower latitudes, the wind has a lot of structure and average speeds of $\approx$

400km/sec. The density (bottom trace) has been corrected for a radial dependence by multiplying by r^2. This scaled density is basically anticorrelated with the speed, being low in the fast wind and highly variable, like the speed, in the slow wind (where high density peaks correlate with low speed minima). The vertical lines show the range of latitudes ($\pm 7.25°$) surveyed by previous in-ecliptic spacecraft and indicate the enormous increase in latitude coverage made possible by Ulysses.

Fig. 14. Variation of solar wind temperature with distance and latitude [18]. The isotropic proton temperature is plotted for essentially the first half of the mission during which the spacecraft traveled from 1.5 to 5.4 AU at low latitudes and then returned inward at increasing south latitudes (indicated in the upper scale), finally passing over the south pole. In the slow wind, the average temperature remained steady at $\approx 5 \times 10^4$ K. (Before measurements were made in the outer heliosphere, it was considered likely that the temperature would decrease adiabatically like $r^{-4/3}$. However, it was found that the wind was being continuously heated by slow stream- fast stream compressions.) As the latitude increased, T rose monotonically in phase with the speed. This correlation between speed and temperature persists both in the ecliptic, where it is well documented, and at high latitude and is a characteristic feature of the solar wind generally.

Fig. 15. Coronal temperature and solar wind abundances and speed [20]. The three parameters are plotted over an interval of slightly more than one solar rotation after Ulysses left the ecliptic headed southward and was alternately encountering slow low latitude wind and fast high latitude wind (because of the tilt of the sun's magnetic dipole relative to its rotation axis). The dashed trace shows the speed of the wind as observed by the α particles rather than protons (the SWICS instrument detects the heavier solar wind ions by design). The other two traces, which are highly correlated, represent the coronal temperature as derived from two charge states of Oxygen (O^{6+} and O^{7+}) and the relative abundances of magnesium to oxygen (Mg/O). The temperature is obtained by modeling conditions in the corona at an altitude at which the degree of ionization is fixed and thereafter remains constant during the solar wind outflow (called the freezing-in temperature). It is found that both the T_O and Mg/O are different in the slow and fast winds being high in the slow wind and low in the fast wind. (Recall that the temperature of the fast wind itself, as distinct from the coronal temperature, is high.)

Fig. 16. The effect of ionization potential /time on heavy ion abundances [20]. The relative abundances of solar wind heavy ions is shown as a function of ionization time in seconds, equivalent to the first ionization potential in volts. The y axis is the ratio of the ion abundance (X) to that of Oxygen normalized to the same ratio in the photosphere, i.e. , (X/O/(X/O photosphere). The ions are identified along the x-axis (Mg through He). The upper dashed line passes through the abundances as found in the slow (inter-stream) wind below an ionization time of 10 sec which is distinct from the abundances in the fast (coronal hole) wind through which the lower dashed line has been drawn. The presence of the First Ionization Potential or FIP effect in the two winds is surprising having been seen previously in energetic particles accelerated at low altitudes in the solar chromosphere.

Fig. 17. Radial component of the magnetic field [21]. The radial field component, B_R, adjusted for radial distance by multiplying by the square of the corresponding distance, r, is plotted as a function of time with latitude given along the top scale. The data were taken when the spacecraft proceeded rapidly from the south to the north poles. The notable features are the change in polarity from -3.2 nT in the south to 3.1 nT in the north hemisphere and the relative constancy of the data above $\pm 20°$. Prior to these measurements, it was expected that the field strength would increase toward the poles because of the dominance of the sun's dipole magnetic field near solar maximum. Instead, as shown, the radial component is independent of latitude. Comparisons with simultaneous measurements in the ecliptic show that this result cannot be caused by a time variation. Since $r^2 B_R$ is basically a measure of solar magnetic flux, the independence of magnetic flux with latitude is implied in the solar wind although not at the sun. Reconciliation of the fluxes at the sun and in the wind implies that the enhanced magnetic pressure in the solar polar regions forces the wind to flow equatorward as well as outward until a magnetic equilibrium is established at a distance estimated to be 5 solar radii. The flux measurements imply a polar magnetic field at the sun of ≈ 7 gauss (7×10^{-4} Tesla).

Fig. 18. Solar wind magnetic field parameters from pole to pole [29]. Three magnetic field parameters are shown as a function of latitude. The top panel contains the field latitude or north-south angle, which should be zero according to the Parker model. This angle has been found to be zero on average in the ecliptic and is now seen to also be zero on average at all latitudes. The middle panel contains the observed and predicted spiral field angles. The two maxima at which the observed angles approach 180° and 360° show the tendency for more radially-directed fields at high latitudes. A tendency for the observed angles to lie slightly above the modeled Parker angles can also be seen. The bottom panel is the observed field magnitude and a reminder that the field strengths are continually changing with distance from the sun.

Fig. 19. Alfvén waves observed at high latitude in the fast wind. The upper three panels contain the components of the magnetic field and solar wind velocity in the radial, tangential (azimuthal) and north-south directions respectively. The bottom panel shows scalar values of the speed and field magnitude. The two middle panels show that the transverse field - velocity components are highly correlated (making it difficult to distinguish between them). The ratio of the field variations to those in the velocity are as predicted by the measured density and the Alfvén (Walén) relation for waves. The field magnitude and speed are relatively constant and uncorrelated with the variations in direction as is also characteristic of Alfvén waves. The fact that the variations are stronger in the transverse components implies that the waves tend to be propagating radially. The in-phase correlation between the field and velocity implies that the waves are propagating opposite to the ambient field direction. Since these data were obtained in the south hemisphere in an inward-directed field, the waves are propagating outward away from the sun.

Fig. 20. Cross correlation coefficients showing the presence of Alfvén waves in both polar regions. The correlation coefficients for the two transverse components of the field

and velocity are shown as a function of time with latitude along the top scale. As the spacecraft travels toward high latitudes, the coefficients increase to values approaching 0.9 in both hemispheres. The signs of the coefficients change from positive to negative during the rapid latitude scan in 1995 consistent with the change in field polarity and with outward-propagating waves in both hemispheres. Near the ecliptic, the correlations are poor and the average coefficients are essentially zero.

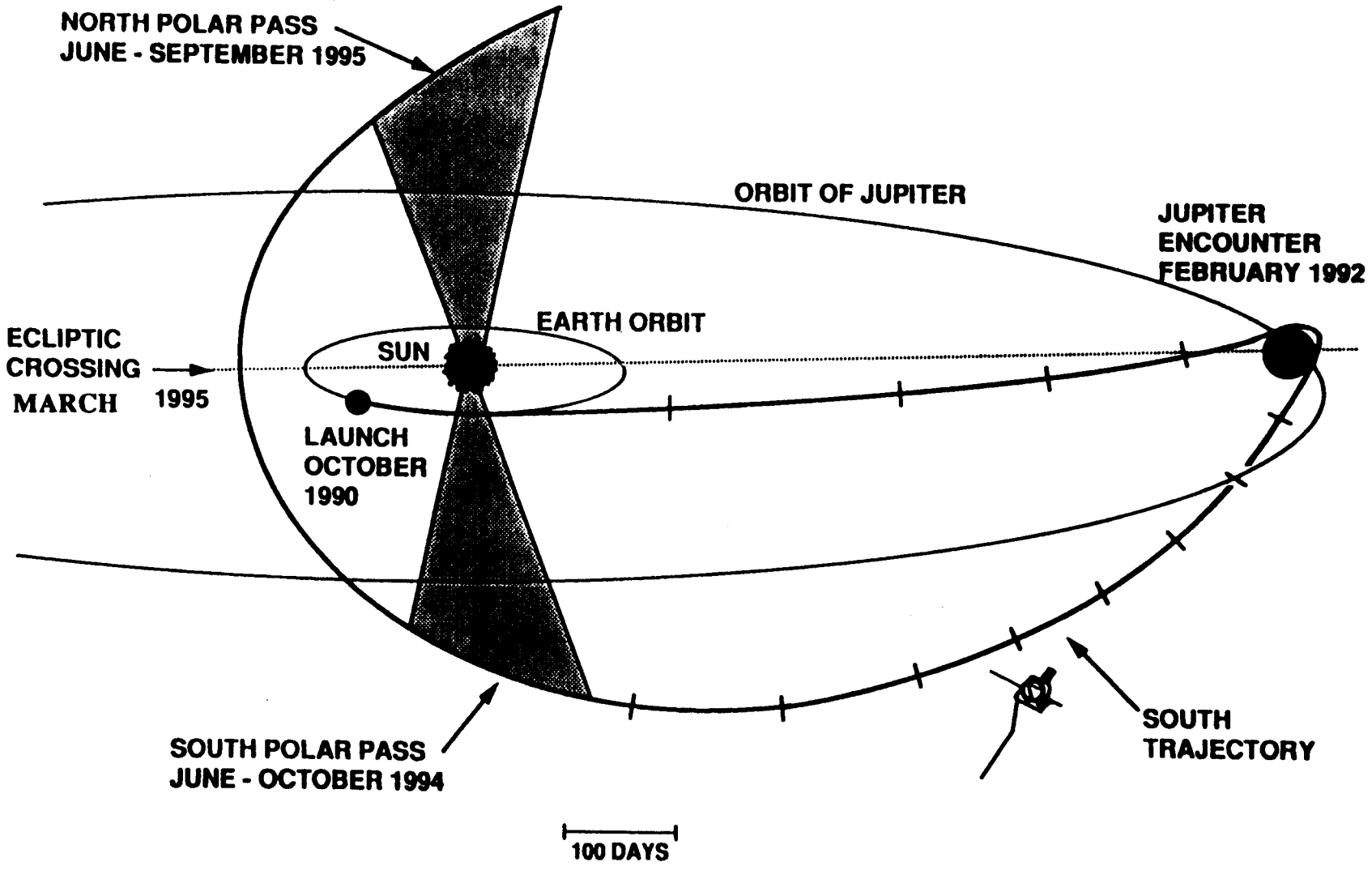
NORTH POLAR PASS
JUNE - SEPTEMBER 1995
ORBIT OF JUPITER
JUPITER
ENCOUNTER
FEBRUARY 1992
EARTH ORBIT
ECLIPTIC
CROSSING
MARCH 1995
SUN
LAUNCH
OCTOBER
1990
SOUTH POLAR PASS
JUNE - OCTOBER 1994
SOUTH
TRAJECTORY
100 DAYS

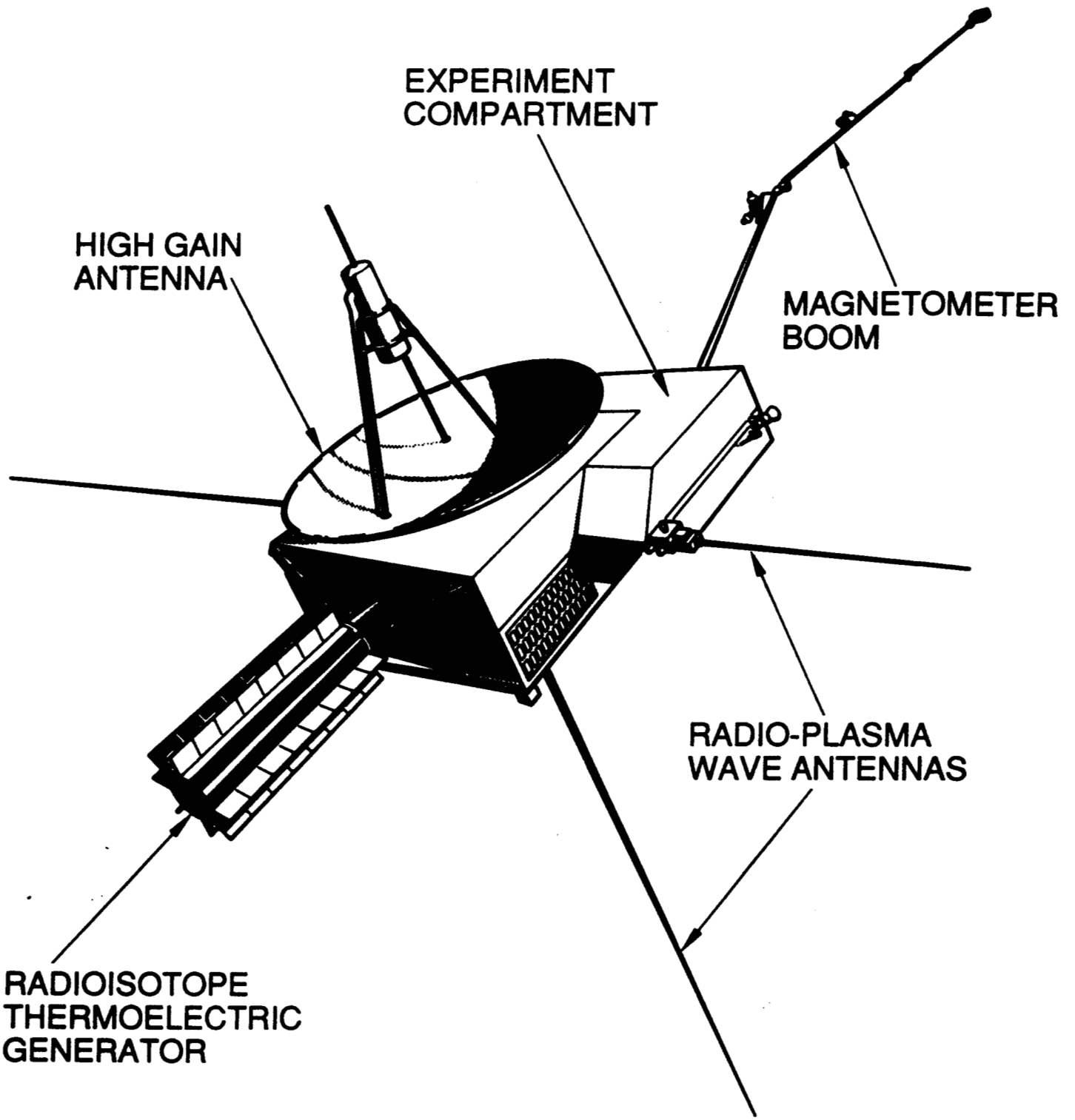
EXPERIMENT
COMPARTMENT
HIGH GAIN
ANTENNA
MAGNETOMETER
BOOM
RADIO-PLASMA
WAVE ANTENNAS
RADIOISOTOPE
THERMOELECTRIC
GENERATOR

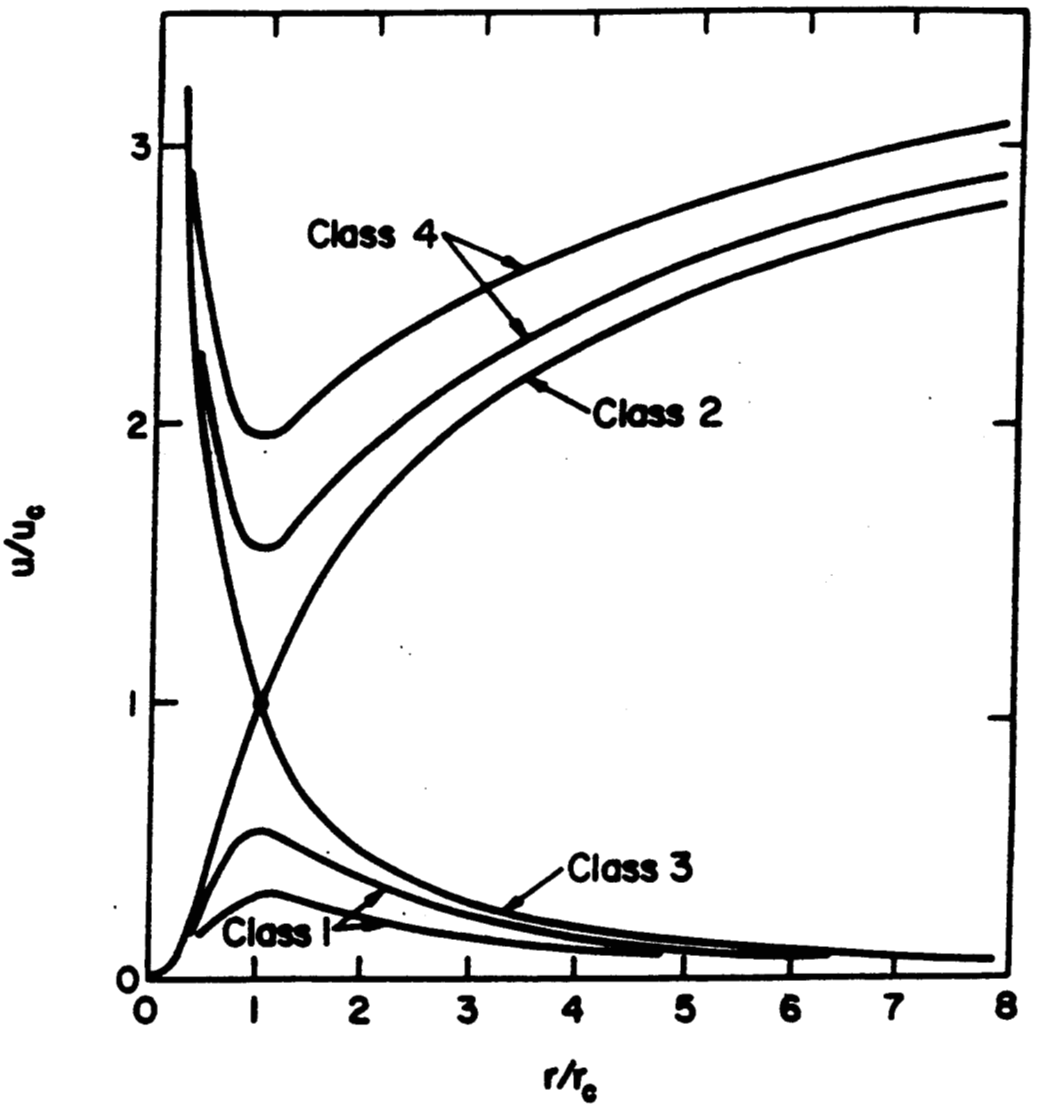

$$r_c = \frac{GM_\odot m}{4kT} \qquad u^2(r_c) = u_c^2 = \frac{2kT}{m}$$

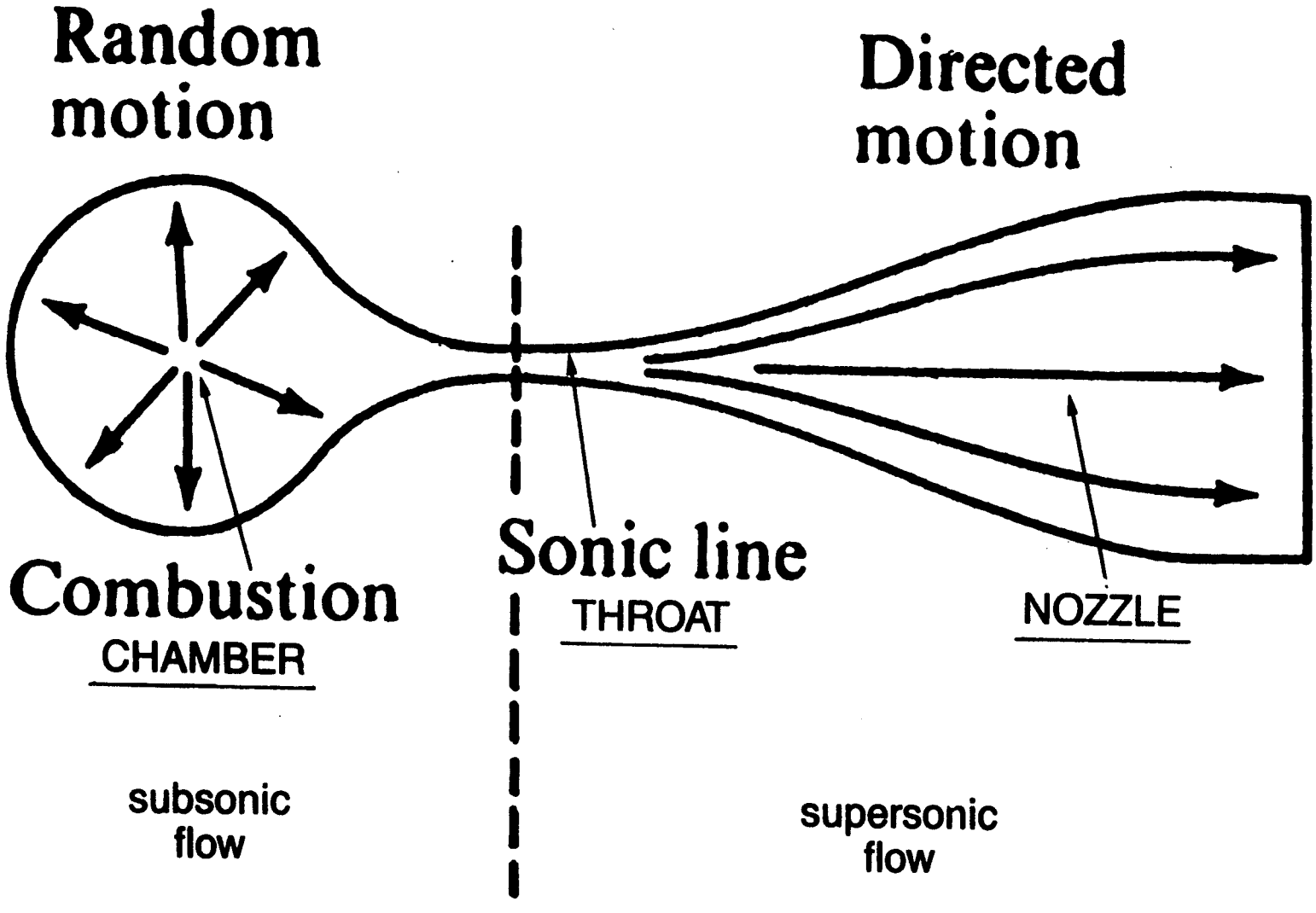
Random motion
Directed motion
Combustion CHAMBER
Sonic line THROAT
NOZZLE
subsonic flow
supersonic flow

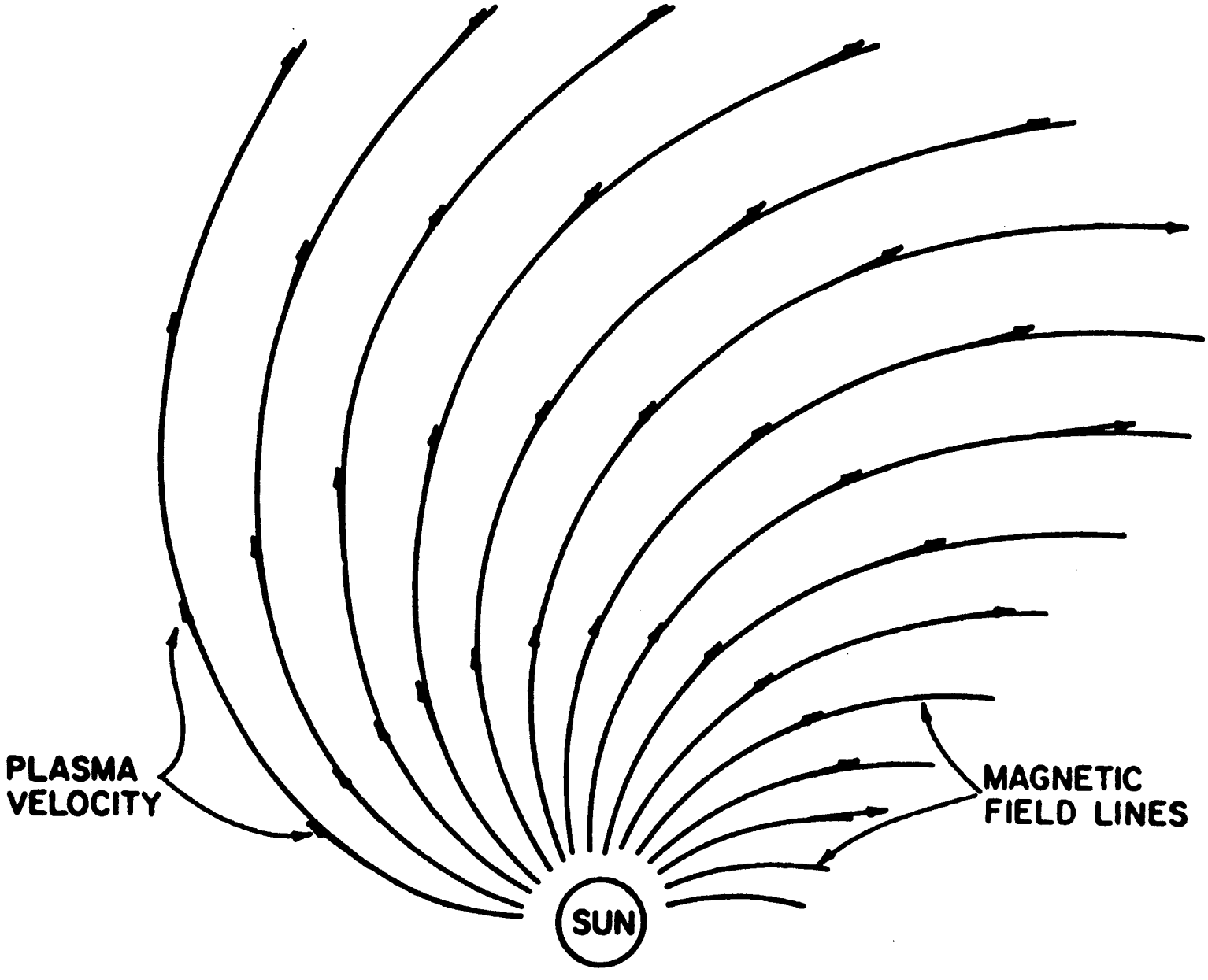
PLASMA
VELOCITY
SUN
MAGNETIC
FIELD LINES

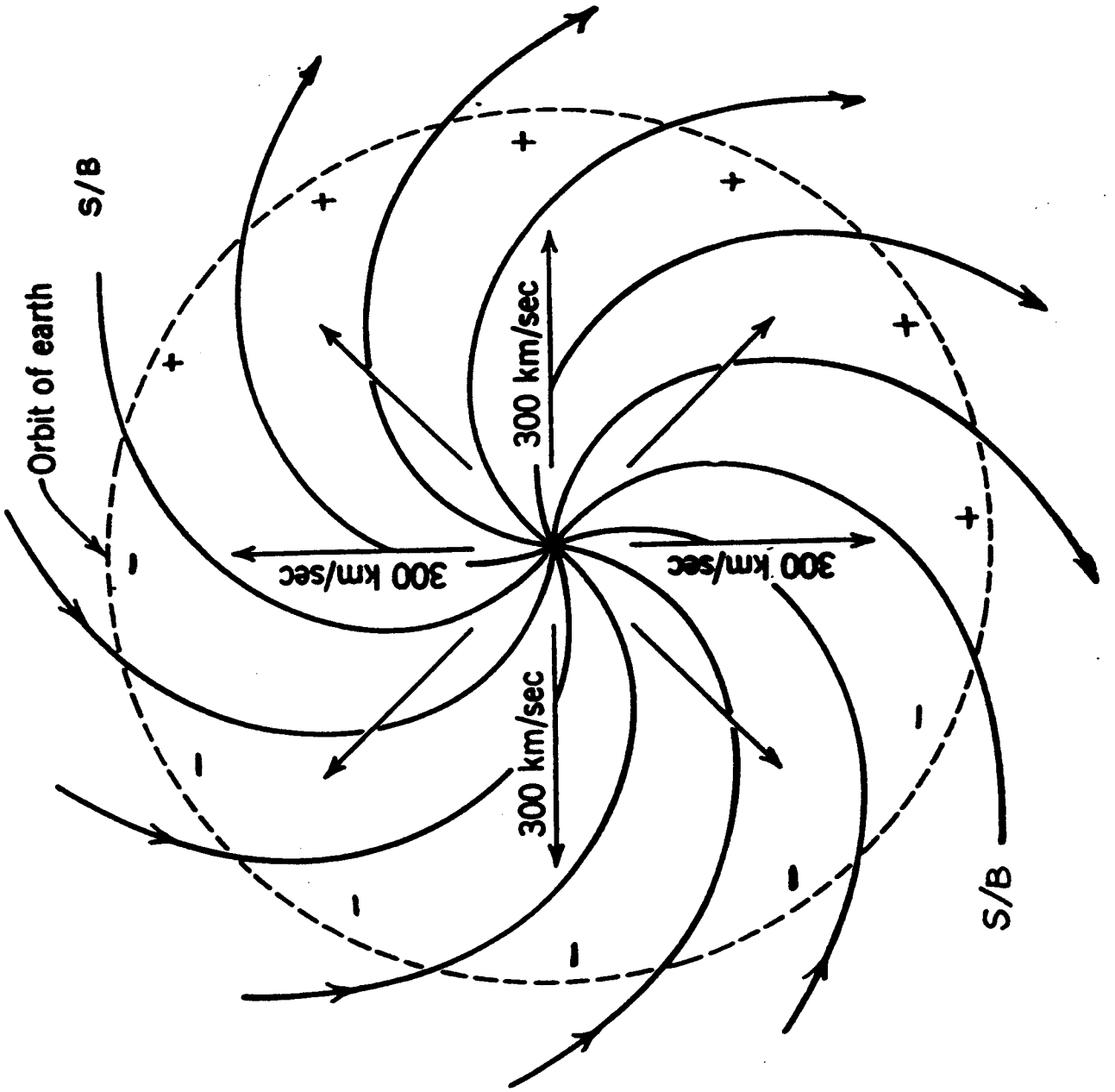
Orbit of earth
S/B
300 km/sec
300 km/sec
300 km/sec
300 km/sec
S/B

INTERPLANETARY SECTOR STRUCTURE

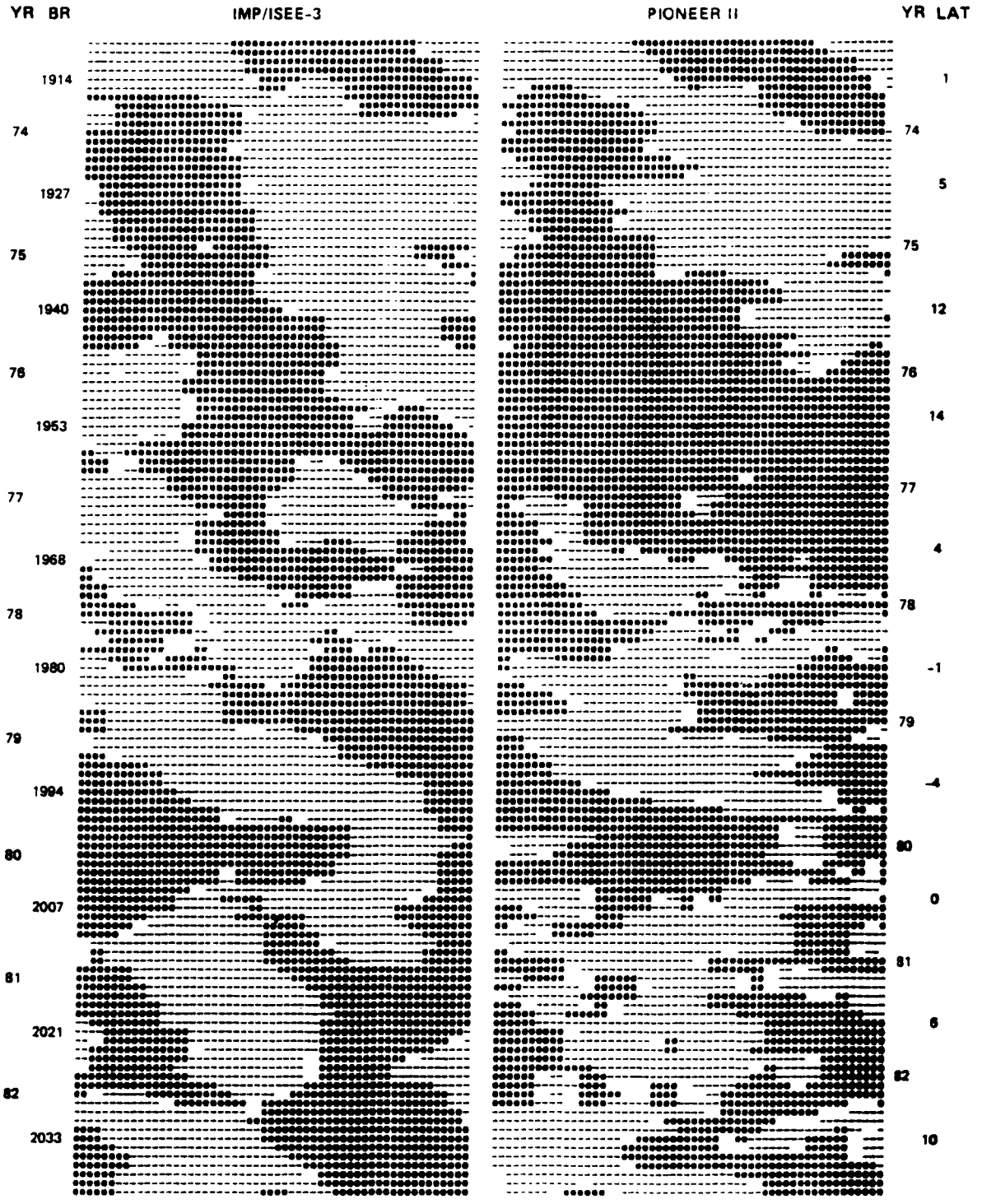

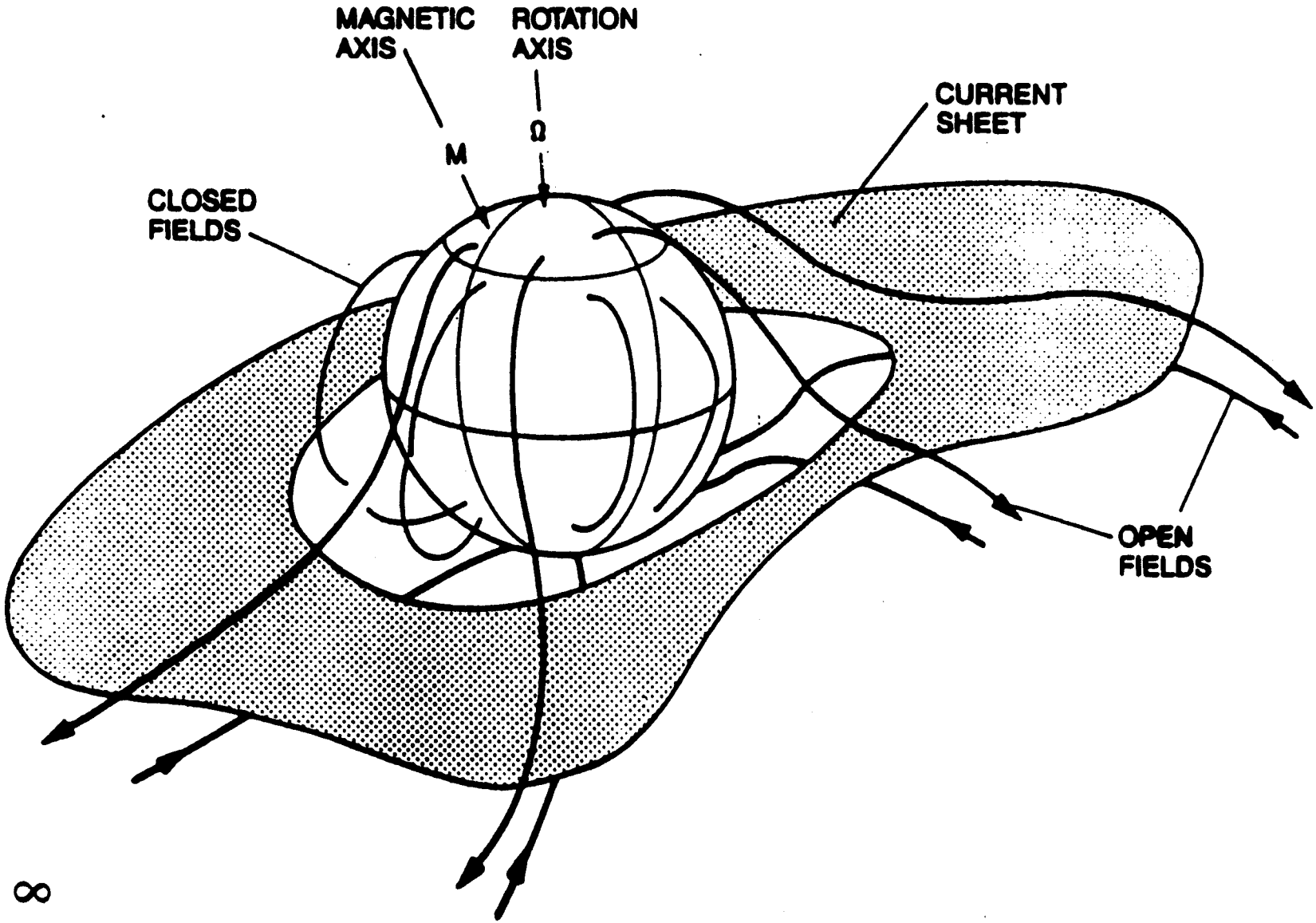
MAGNETIC AXIS
ROTATION AXIS
Ω
M
CURRENT SHEET
CLOSED FIELDS
OPEN FIELDS

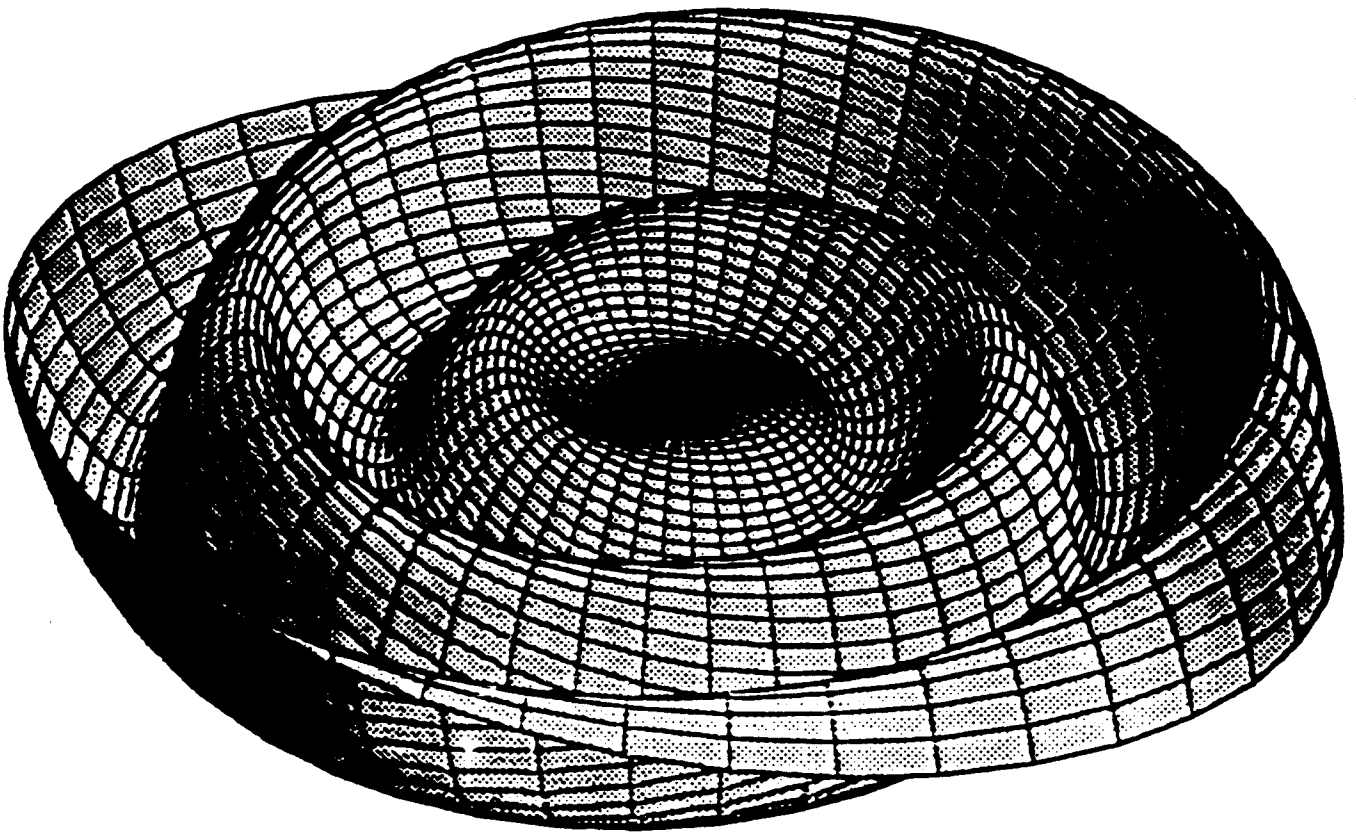

HYPERBOLIC (RECIPROCAL) SPIRAL

$$r\,\Phi = a$$

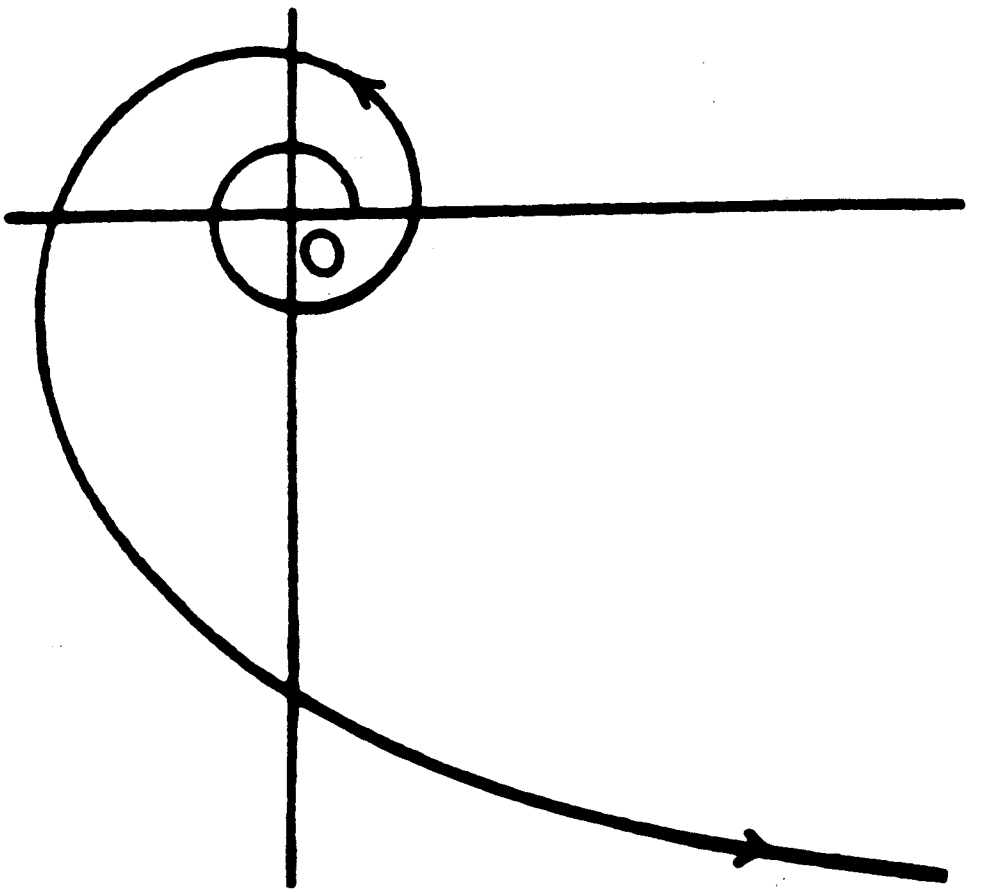

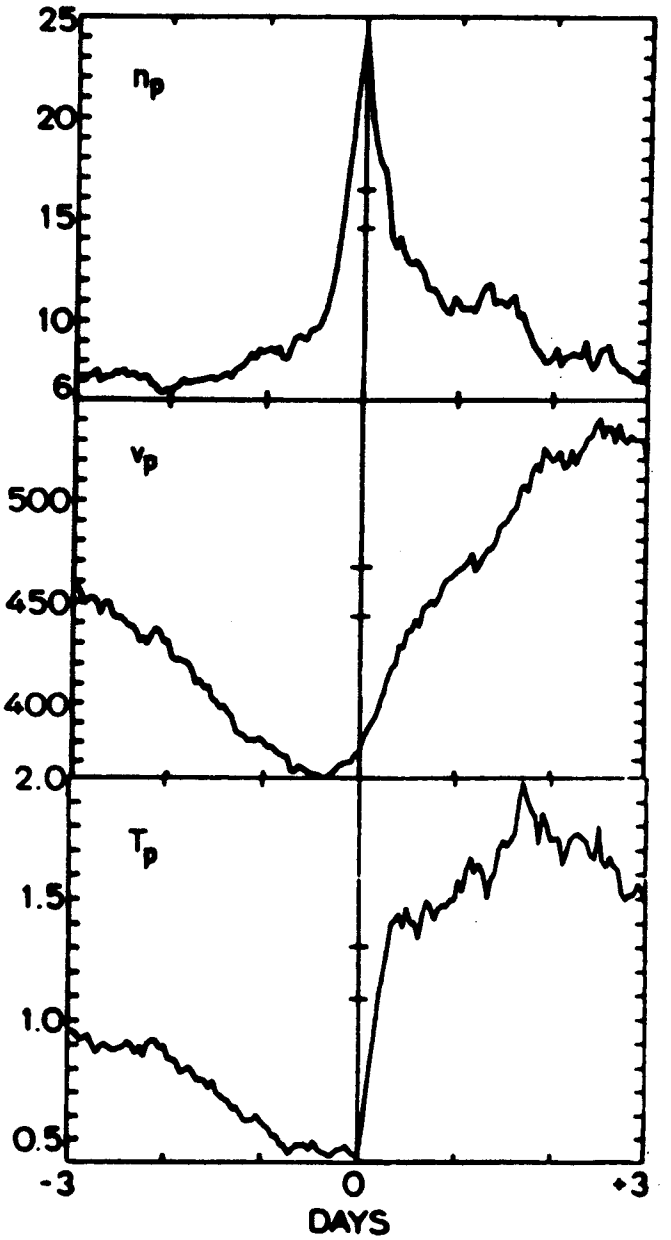
25
20
15
10
6
n_p
500
450
400
v_p
2.0
1.5
1.0
0.5
T_p
-3
0
+3
DAYS

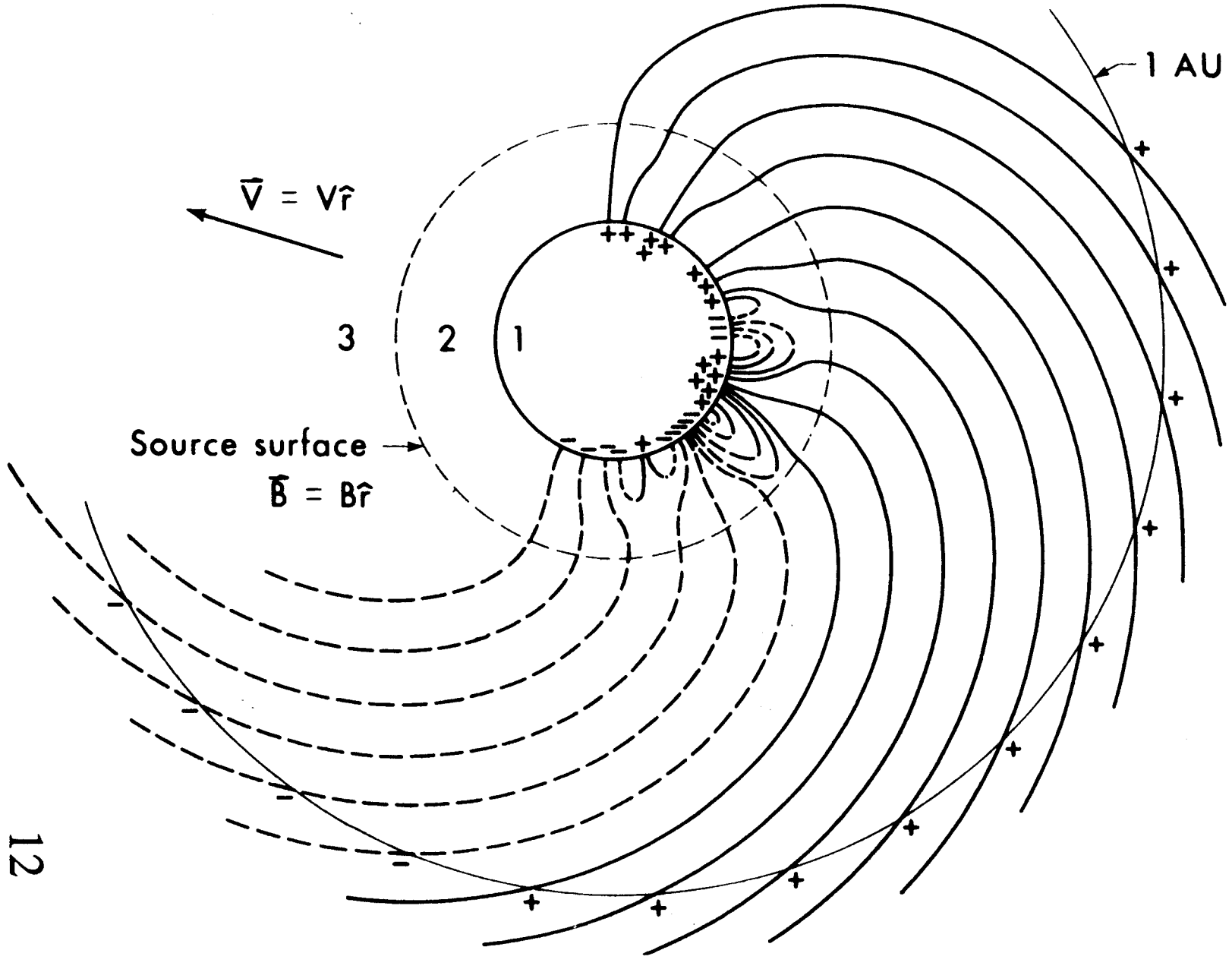
1 AU
$\vec{V} = V\hat{r}$
3
2
1
Source surface
$\vec{B} = B\hat{r}$

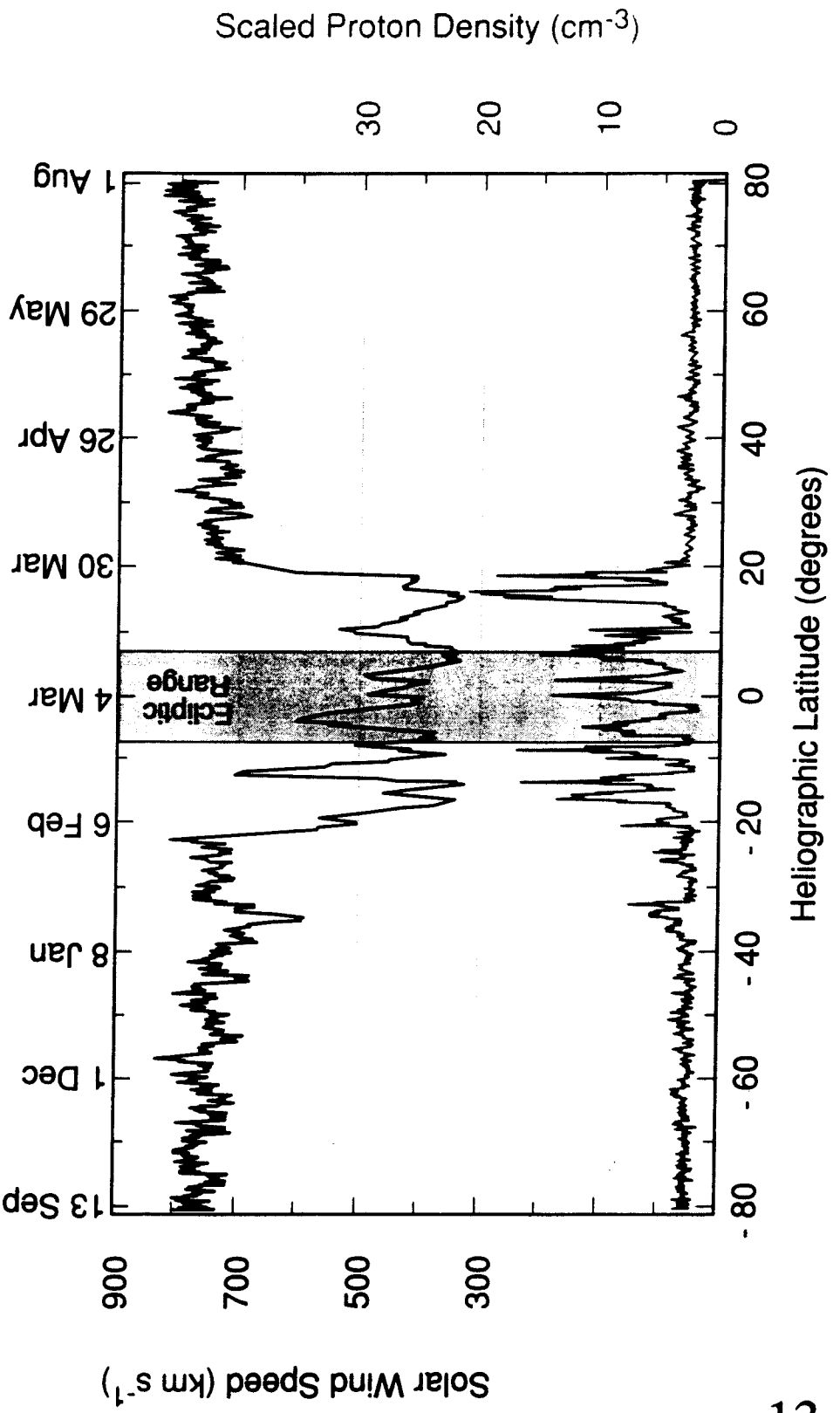
Scaled Proton Density (cm-3)
30
20
10
0
1 Aug
29 May
26 Apr
30 Mar
4 Mar
Ecliptic Range
6 Feb
8 Jan
1 Dec
13 Sep
80
60
40
20
0
- 20
- 40
- 60
- 80
Heliographic Latitude (degrees)
900
700
500
300
Solar Wind Speed (km s-1)

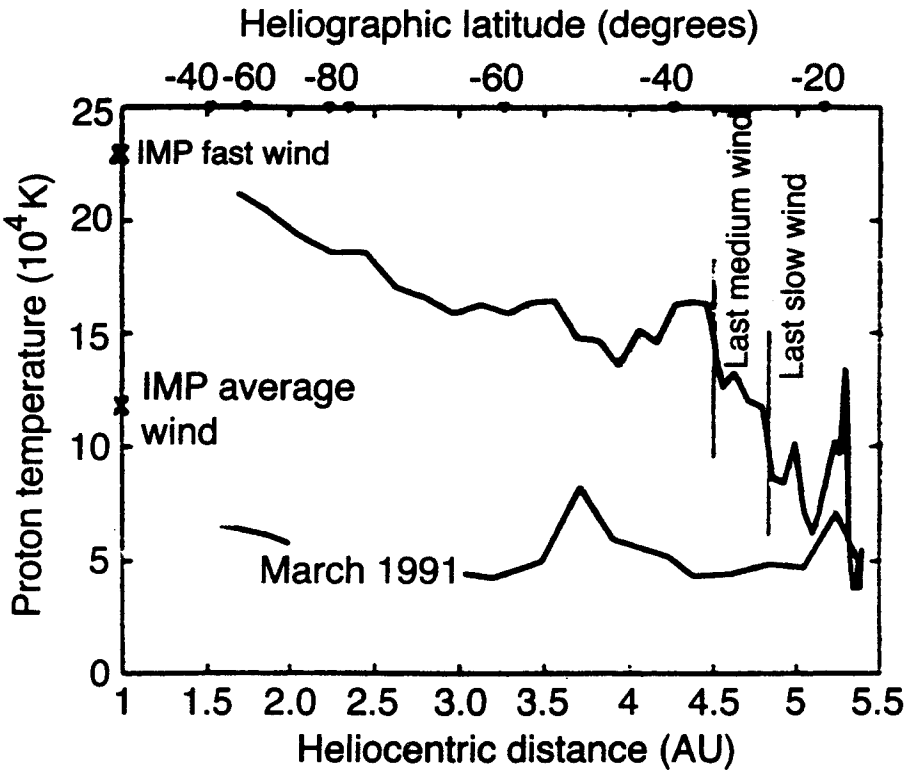
Heliographic latitude (degrees)
-40 -60 -80 -60 -40 -20
25
20
15
10
5
0
IMP fast wind
IMP average wind
Last medium wind
Last slow wind
March 1991
Proton temperature (10^4 K)
1 1.5 2.0 2.5 3.0 3.5 4 4.5 5 5.5
Heliocentric distance (AU)

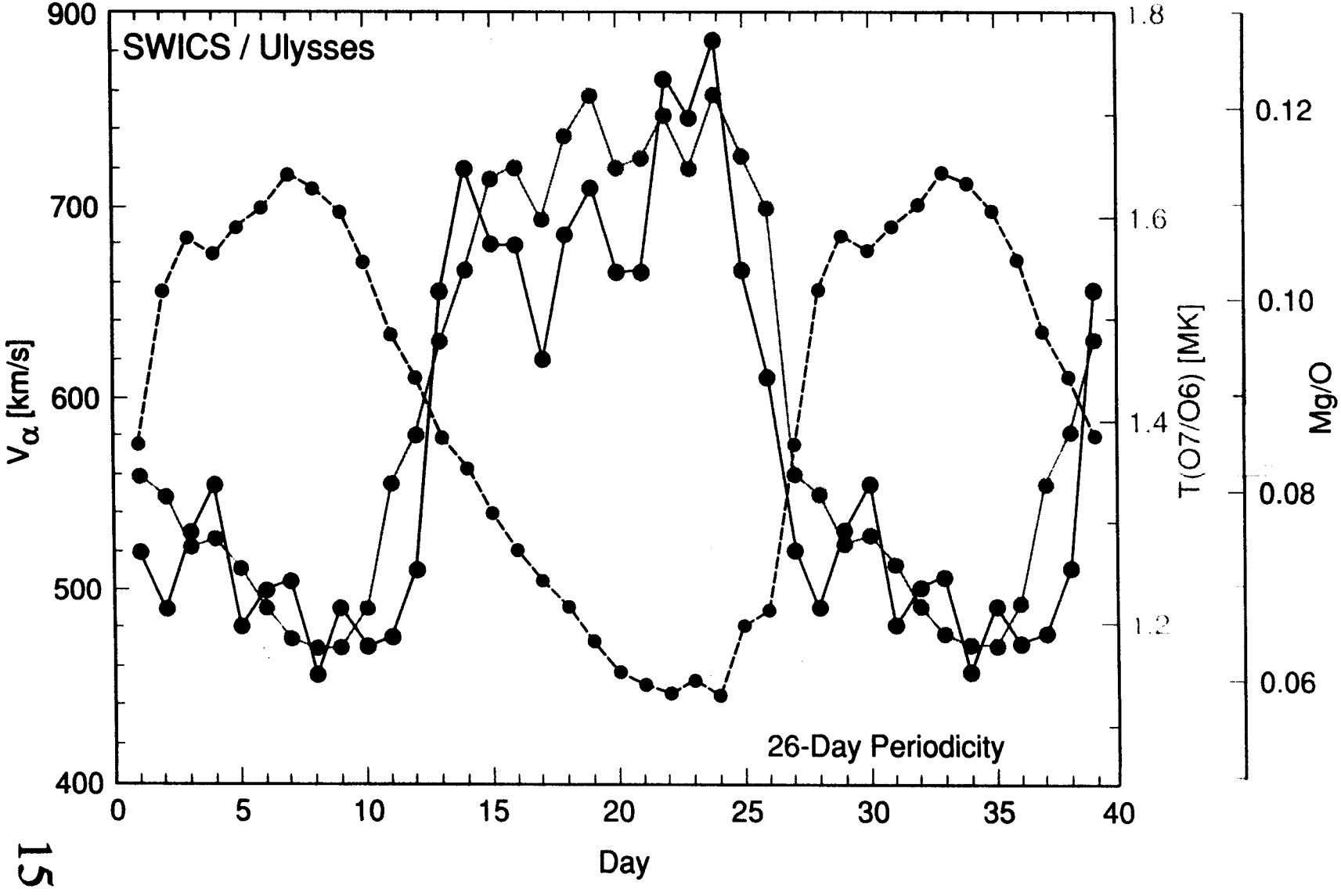
SWICS / Ulysses
900
700
600
500
400
V_α [km/s]
1.8
1.6
1.4
1.2
T(O7/O6) [MK]
0.12
0.10
0.08
0.06
Mg/O
0
5
10
15
20
25
30
35
40
Day
26-Day Periodicity

10
1
(X/O) / (X/O)Photosphere
Solar Wind (Interstream)
SW from Coronal Holes
Mg
Si
Fe
S
Xe
KrC
N
O
Ar
Ne
He
0.1
1.0
10.0
100.0
First Ionization Time [s]

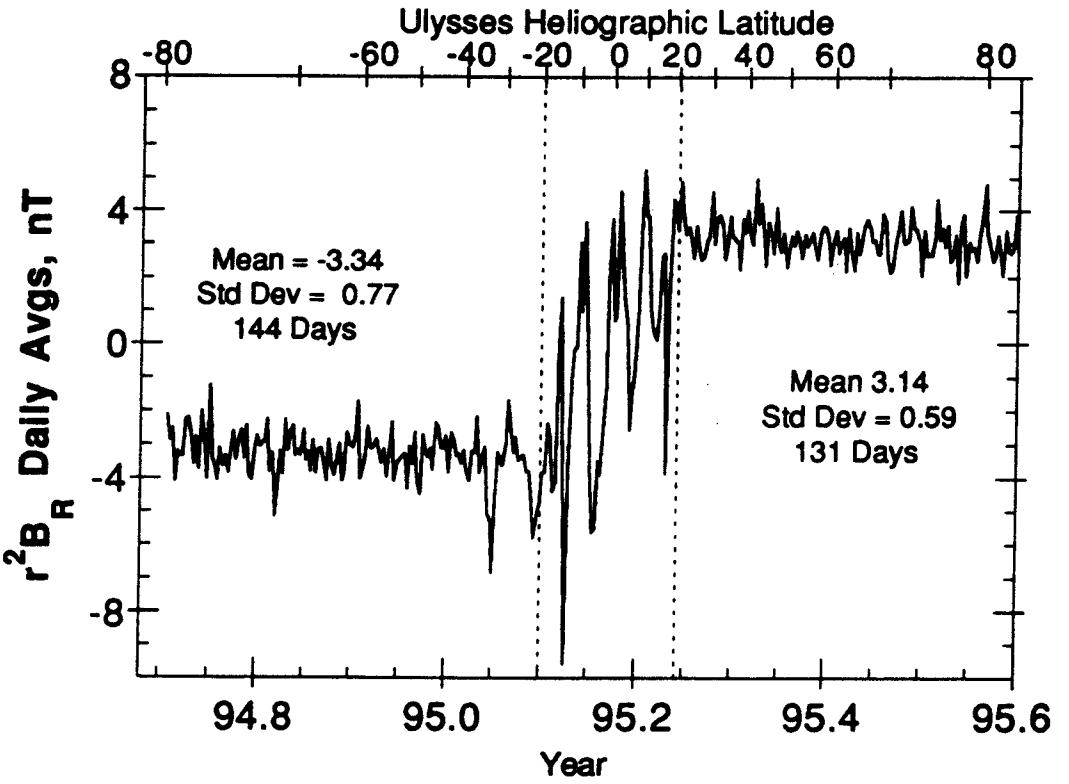
Ulysses Heliographic Latitude
-80
-60
-40
-20
0
20
40
60
80
8
4
0
-4
-8
r^2B_R Daily Avgs, nT
Mean = -3.34
Std Dev = 0.77
144 Days
Mean 3.14
Std Dev = 0.59
131 Days
94.8
95.0
95.2
95.4
95.6
Year

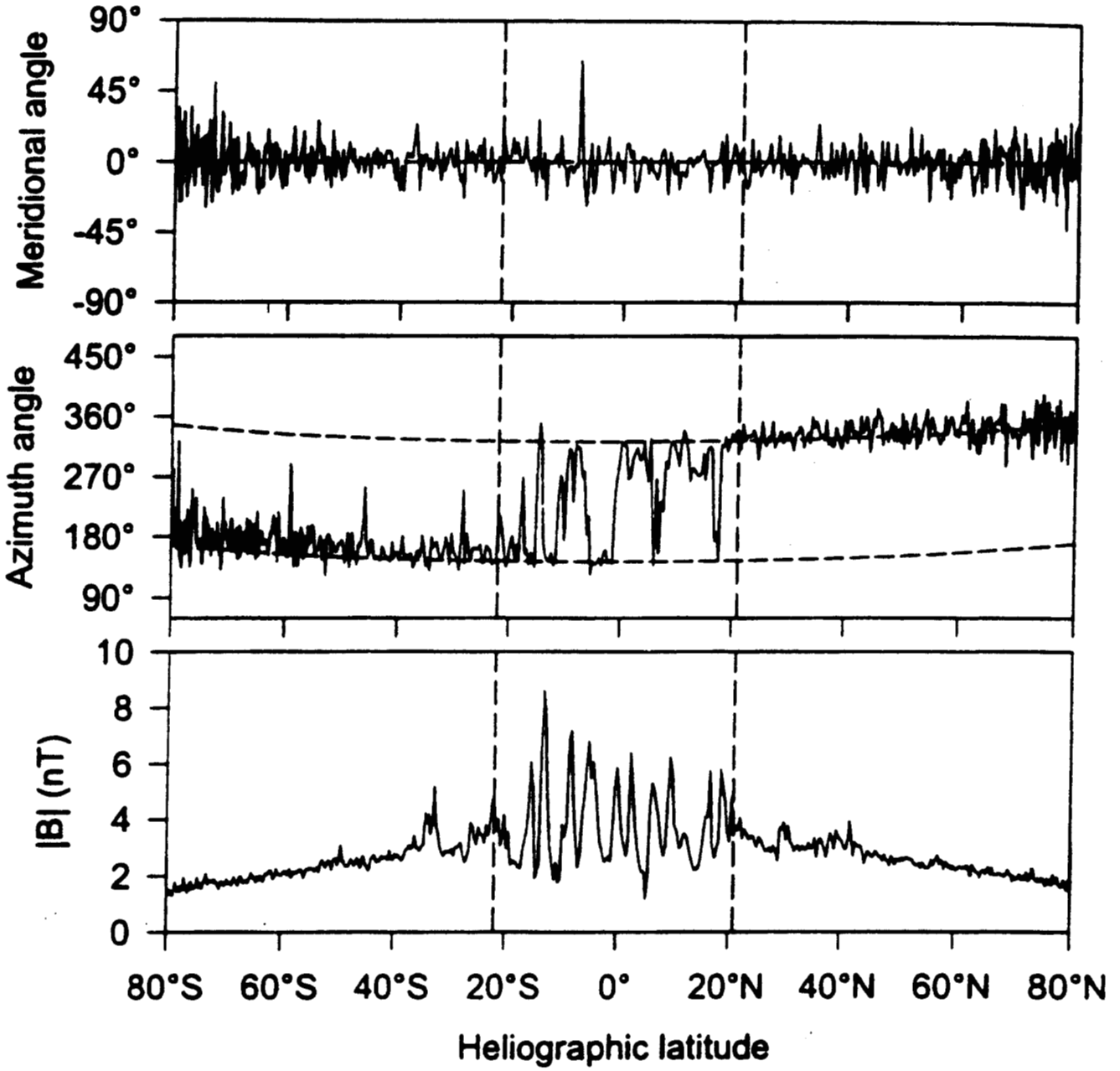
Meridional angle
90°
45°
0°
-45°
-90°
Azimuth angle
450°
360°
270°
180°
90°
|B| (nT)
10
8
6
4
2
0
80°S
60°S
40°S
20°S
0°
20°N
40°N
60°N
80°N
Heliographic latitude

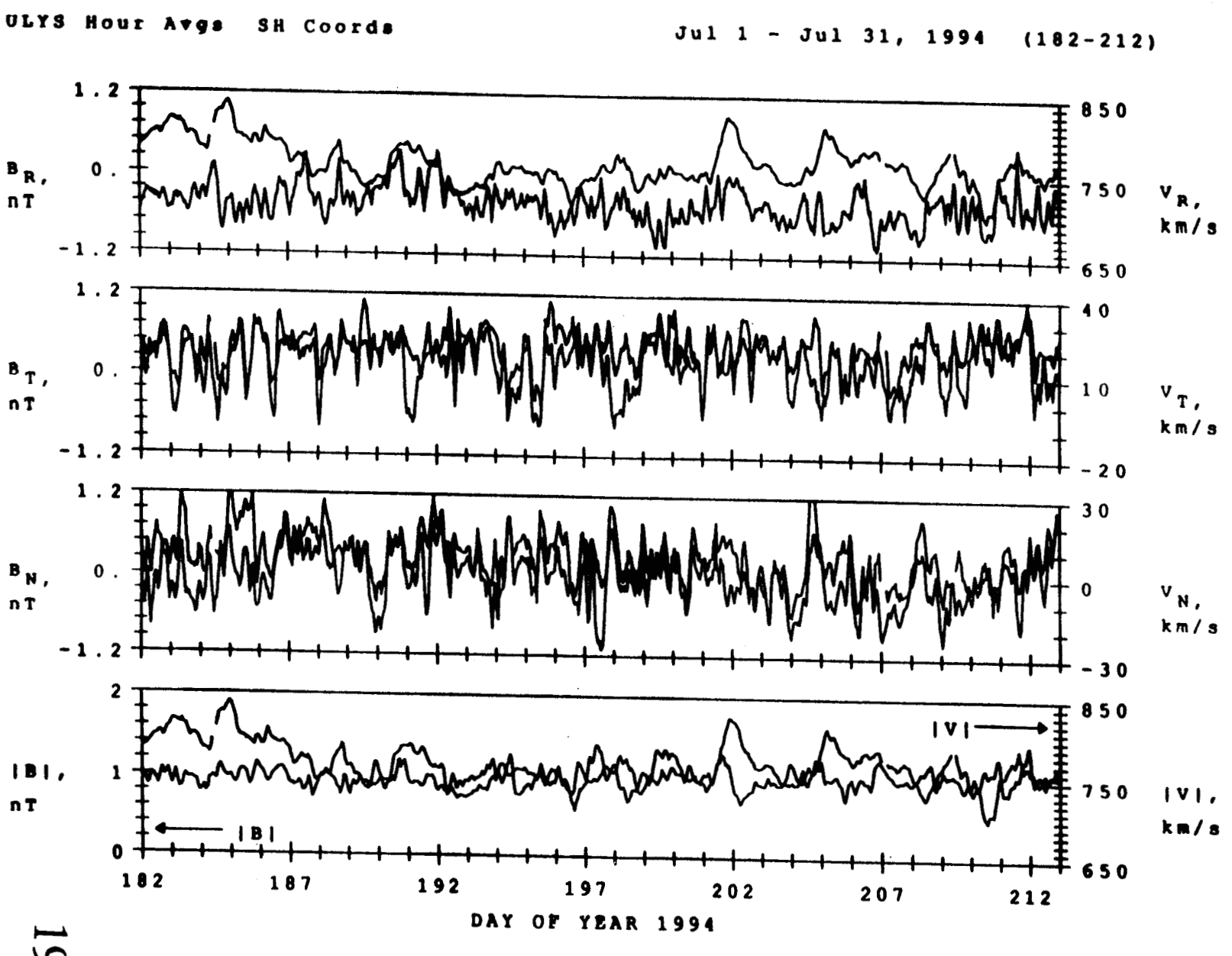
ULYS Hour Avgs SH Coords
Jul 1 - Jul 31, 1994 (182-212)
1.2
0.
-1.2
B_R, nT
850
750
650
V_R, km/s
B_T, nT
40
10
-20
V_T, km/s
B_N, nT
30
0
-30
V_N, km/s
2
1
0
|B|, nT
|V|
|B|
|V|, km/s
182
187
192
197
202
207
212
DAY OF YEAR 1994

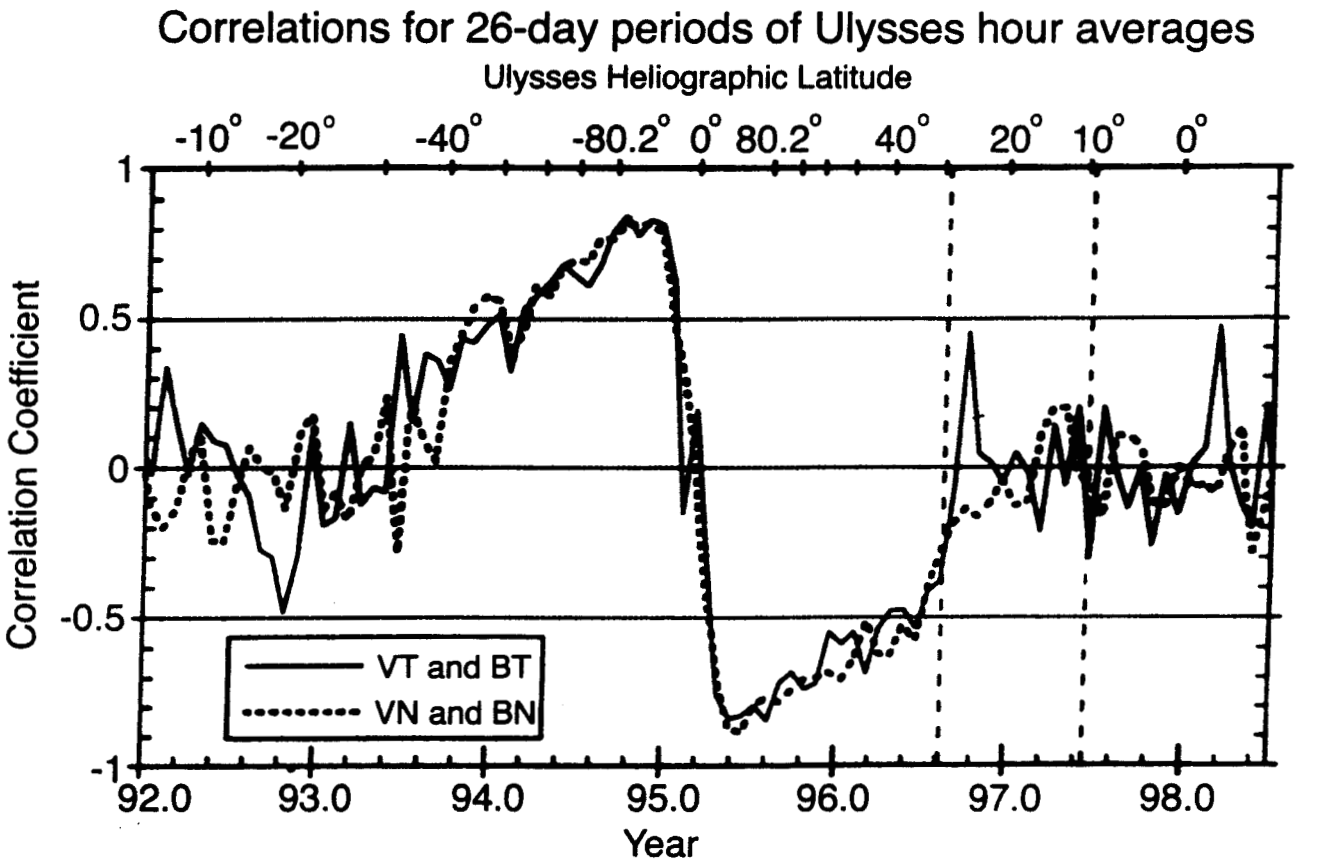
Correlations for 26-day periods of Ulysses hour averages
Ulysses Heliographic Latitude
-10° -20° -40° -80.2° 0° 80.2° 40° 20° 10° 0°
1
0.5
0
-0.5
-1
Correlation Coefficient
VT and BT
VN and BN
92.0
93.0
94.0
95.0
96.0
97.0
98.0
Year